Indian J Radio & Space Phys, Vol. 13, No. 4, pp. 109-138
AUGUST 1984
CODEN : IJRSAK ISSN : 0367-8393
13(4) 109-138 (1984)

INDIAN JOURNAL OF RADIO & SPACE PHYSICS

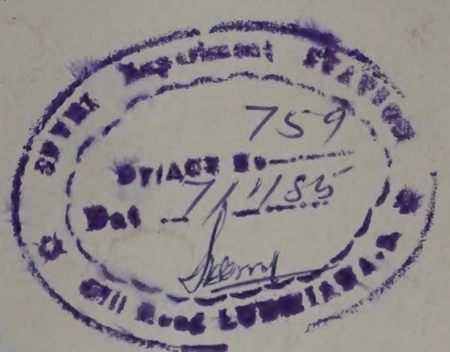

Published by
PUBLICATIONS & INFORMATION DIRECTORATE, CSIR, NEW DELHI
in association with
THE INDIAN NATIONAL SCIENCE ACADEMY, NEW DELHI

Indian Journal of Radio & Space Physics

Published by the Publications & Information Directorate, CSIR, Hillside Road, New Delhi 110012

Editor-in-Chief: Y R Chadha

The Indian Journal of Radio & Space Physics is issued bimonthly.

The Directorate assumes no responsibility for the statements and opinions advanced by contributors. The editorial staff in its work of examining papers received for publication is assisted, in an honorary capacity, by a large number of distinguished scientists.

Communications regarding contributions for publication in the Journal should be addressed to the Editor, Indian Journal of Radio & Space Physics, Publications & Information Directorate, CSIR, Hillside Road, New Delhi 110012.

All correspondence regarding reprints, Journal copies, subscriptions, renewals, claims for missing numbers and advertisements, should be addressed to: The Sales & Distribution Officer, Publications & Information Directorate, CSIR, Hillside Road, New Delhi 110012. Payments may be sent by money order, cheque, bank draft or postal order marked payable to PUBLICATIONS & INFORMATION DIRECTORATE, NEW DELHI 110012.

Claims for missing numbers of the Journal will be allowed only if received within 3 months of the date of issue of the Journal plus the time normally required for postal delivery of the Journal and the claim.

Annual Subscription: Rs 100.00 £19.00 $ 34.00 **Single Copy**: Rs 20.00 £3.80 $ 6.80

50% Discount is admissible to research workers and students and 25% discount to non-research individuals, on annual subscription.

Indian Journal of Radio & Space Physics

VOLUME 13 NUMBER 4 AUGUST 1984

CONTENTS

Indian Journal of Radio & Space Physics
Vol. 13, August 1984, pp. 109-111

Infrasonic Observations at Antarctica

R VENKATACHARI, A SEN GUPTA & A K SAHA
National Physical Laboratory, New Delhi 110012
and
B J SRIVASTAVA
National Geophysical Research Institute, Hyderabad 500007

Received 22 *February* 1984; *revised received* 25 *June* 1984

Microbarograph observations at Antarctica by the Indian scientific expedition of the winter of 1982-83 are reported. The general features are described and specific effects of magnetic disturbances as compared to observations taken in India are highlighted. Some earthquake and explosion effects are also indicated.

1 Introduction

The second Indian scientific expedition team to Antarctica (1982-83) set up a base camp at 69°59'S, 11°55'E and carried out various experiments with ground based instruments for a period of nearly 40 days from 8 Jan. 1983 to 18 Feb. 1983. One microbarograph was set up by National Physical Laboratory (NPL) group primarily for studying magnetic disturbance effects near the auroral zone, for comparing the earlier findings[1] with microbarographs that are in operation for several years at NPL, New Delhi, and at National Geophysical Research Institute (NGRI), Hyderabad. The microbarographs at Delhi, Hyderabad and Antarctica are of identical types, the elements being condenser microphone type with a frequency response of 0.001 Hz to 2 Hz.

In this paper, we are reporting the general features of infrasonics that are observed at the Antarctica as compared to what are observed at the Indian stations. The infrasonics correlated with magnetic storms and bays (recorded by the Hyderabad magnetic observatory) are especially studied. Pressure fluctuations, apparently associated with earthquakes/explosions of ocean-bed origin are also illustrated.

The observations reported here are our initial efforts in the second Antarctica expedition and are for a limited period of 40 days only. This study justifies the need for future studies over longer periods of time.

2 Infrasonic Records on Normal Days

Antarctica is an icy continent and the normal daytime temperature during summer is around 0 to $-6°C$, nighttime temperature being around $-6°$ to $-12°C$. During the later part of the period of observation, the sunset occurred around 2200 hrs U T and the sunrise around 0200 hrs U T. A representative daytime record of infrasonic pressure is shown in Fig. 1. The daytime variation is within ± 200 μ bar whereas for a low latitude station[2], it is of the order of ± 1000 μ bar. Since the insolation received from the sun is small, convective heating and the consequent daytime turbulence are not as intense as in the tropics. Daytime and nighttime records are not very different, except that the amplitudes are sometimes reduced during night.

3 Infrasonics and Magnetic Activity

During magnetic storms, infrasonic pressure variations in Antarctica are found to be quite disturbed as compared to midlatitude in conformity with the measurements made in the Arctic region by earlier workers[3].

From our observations in India on infrasonic pressure variations[1] at Delhi and Hyderabad we had concluded that infrasonic waves generated in the Arctic and Antarctic auroral regions travel down to low latitudes under favourable conditions, with speeds of the order of 500 m/sec. We identified some sinusoidal patterns in the microbarograph associated

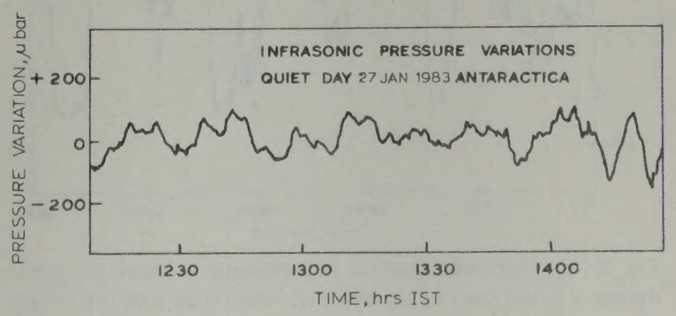

Fig. 1—Infrasonic pressure variation on a quiet day at Antarctica (27 Jan. 1983)

with the substorms. Microbarograph records at Antarctica were especially investigated for the magnetic bay effects. Whenever a substorm was recorded in the Hyderabad magnetograms, sinusoidal oscillations associated with substorms were noted in Antarctica microbarograms, with delay times in the range of 15-60 min. The geomagnetic latitude of our Antarctic station is 62 S, and it is well outside the auroral oval.

We had earlier[1] interpreted (following Wilson[4]) the substorm associated infrasonic waves as due to Joule heating in supersonic auroral area during polar magnetic substorms. All the 6 substorm cases noted by us were in the same diurnal time zone and occurring in the late afternoon and evening hours. As such the delay time range could not be ascribed to diurnal location changes of the auroral oval[5]. In the absence of information about the exact location and size of the auroral oval during these events, the reason for the observed delay-time range could not be inferred.

One special case with some unusual features is illustrated in Fig. 2 [(a), (b)]. An SSC was recorded at Hyderabad magnetogram at 1544 hrs U T ($H = 49\gamma$) on 9 Jan. 1983. Sinusoidal oscillations, associated with substorms appeared in Antarctic microbarograph records 15 min. later [Fig. 2(a)]. It has been reported[6] that an SSC observed in mid and low latitude can trigger a substorm in auroral station. Fig. 2(b) shows some strong fluctuations in microbarograph records some 3 hr prior to this event. This may or may not be related to the SSC event. Annyhow it is recorded here pending more such observations in future expeditions.

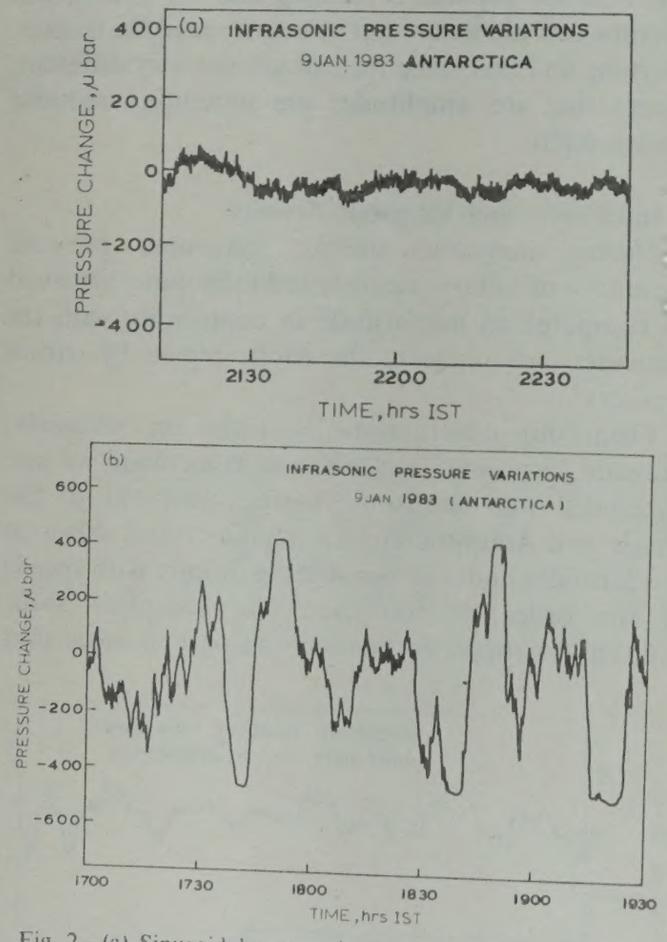

Fig. 2—(a) Sinusoidal pattern in infrasonic pressure variation during a substorm (9 Jan. 1983) in Antarctica and (b) strong fluctuations in infrasonic pressure variations prior to substorm on 9 Jan. 1983

4 Some Special Events

The special nature, topography and location of Antarctica station and the fact that the daytime thermal disturbances observed in lower latitudes are absent, make the observations of special events and interesting features more convenient. We are reporting two specific cases where linkage of infrasonic pressure variation could exist with an earthquake and with some explosion or explosive movement.

4.1 Earthquake Effect

A major earthquake occurred at 2309 hrs U T on 24 Jan. 1983 with the epicentre in the Andaman Sea (lat., 12.95 N; long., 93.4 E) at a depth of 79 km with a

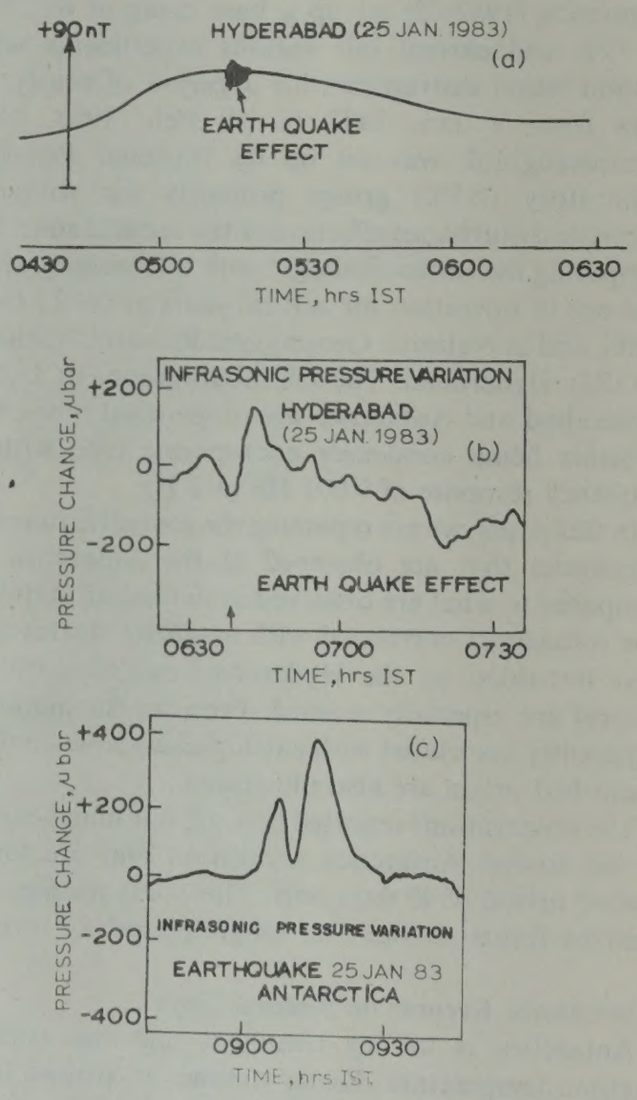

Fig. 3—Earthquake effect recorded on a magnetogram at Hyderabad and its effect on infrasonic pressure variations at Hyderabad and at Antarctica (25 Jan. 1983)

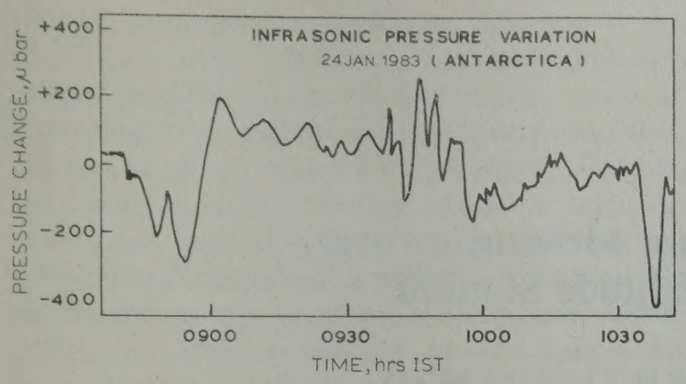

Fig. 4—A special pattern (explosion?) of infrasonic pressure variation at Antarctica (24 Jan. 1983)

magnitude of 6.3 in Richter scale. This is shown as an effect in the magnetogram at Hyderabad.

Fig. 3 shows the microbarograph record at Hyderabad where a peak can be distinguished at 0640 hrs IST on 25 Jan. 1983 corresponding to a delay of about 2 hr which would be expected from a speed of 300 m/sec (expected acoustic speed in the troposphere). The corresponding pattern (with a time delay of 4.5 hr) at Antarctica is also shown in Fig. 3(c). The waveform has apparently been degenerated to a doulbe pulse and the time delay for a distance of the order of 7800 km would correspond to a high speed of 500 m/sec. Perhaps, the propagation was through ocean waves. More observation of this phenomenon is needed to arrive at a definite conclusion.

4.2 An Explosion

Fig. 4 shows a special pattern observed in the Antarctica microbarograph records on the morning of 24 Jan. 1983. Two trains of waves of larger amplitudes separated by a wave train of smaller amplitude are seen. The nature of the disturbance would indicate an explosive event, more likely on the sea bed. In the absence of any specific information, it is not possible to speculate further. As the atmospheric conditions were calm and also similar to any other neighbouring day and no magnetic event was reported, atmospheric origin of this event is ruled out.

Acknowledgement

The authors wish to thank Dr S Z Qasim, Department of Oceanography, Goa, for allowing a berth for these equipments in the Antarctica expedition and Mr V K Raina and other members of the Antarctica expedition party for their active help.

References

1 Srivastava B J, Venkatachari R & Saha A K, *Geophys J R Astron Soc*, **71** (1982) 241.

2 Venkatachari R & Bhartendu, *Indian J Radio & Space Phys*, **8** (1979) 273.

3 Campbell W H, In *Physics of the geomagnetic phenomena*, edited by Matsushita S & Campbell W H (Academic Press, New York) 1967, 860.

4 Wilson C R, *J Geophys Res (USA)*, **74** (1969) 1812.

5 Akasofu S I, *Upper Atmosphere Research in Antarctica*, edited by Lanzerotti L I & Park G G (American Geophysical Union), 1978, 157.

6 Hirasawa T, *Proceedings of the fourth symposium on coordinated observations of the ionosphere and the magnetosphere in the polar regions*, edited by Takesi Nagata (National Institute of Polar Research, Tokyo), 1982, 104.

Indian Journal of Radio & Space Physics
Vol. 13, August 1984, pp. 112-115

Nighttime F-layer Vertical Movements over Indian Low & Midlatitude Stations

P ERNEST RAJ, P C S DEVARA & Bh V RAMANA MURTY
Indian Institute of Tropical Meteorology, Pune 411 005

Received 23 *March* 1984

Nighttime hourly rate of change of $h'F$ is computed for Kodaikanal, Hyderabad and Ahmedabad representing, respectively, the equatorial, low and midlatitude stations in India. Data for several years are considered for examining the nature of nighttime F-layer vertical movements at the above latitudes. Vertical movements at Kodaikanal seem to be controlled by the electrodynamic ($\mathbf{E} \times \mathbf{B}$) effects and those at Ahmedabad are influenced by meridional neutral wind effects. At an intermediate latitude (low midlatitude) station like Hyderabad, the dynamical behaviour of the F-layer could be due to the competing effects of neutral winds, electric fields and diffusion. The observed seasonal variations in nighttime vertical drifts also confirm the above conclusions. The results of the present study are compared with those reported for stations in the American longitudes.

1 Introduction

The study of vertical drift of ionization in the F-region of the ionosphere leads to an understanding of many ionospheric phenomena especially during nighttime. Vertical drifts help in the maintenance of nighttime F-layer[1] and the onset of post-sunset equatorial spread-F seems to be closely associated with the upward-to-downward reversal of motion of the ionosphere in the post-sunset period and also with the speed at which the F-layer moves vertically in the sunset period[2-4].

Vertical drifts after sunset hours could be either due to electrodynamic ($\mathbf{E} \times \mathbf{B}$) effects[5-7] or due to neutral air winds[1,8-11]. Besides these two effects, other phenomena which are thought to be contributing to the height variations and vertical motions are the thermal expansion and contraction[12], ambipolar diffusion[13] and gravity wave effects[14]. It is now generally accepted that $\mathbf{E} \times \mathbf{B}$ drifts are more pronounced at near-equatorial latitudes, whereas meridional neutral winds dominate the motion of the F-region ionization in the middle and high latitudes. The dynamical behaviour of the F-layer at an intermediate latitude (low midlatitude) could be due to the competing effects of electric fields, neutral winds and diffusion[15].

The neutral atmosphere at F-region ionospheric heights is far from static; diurnal heating and cooling by the sun induce pressure gradients that drive the neutral air to produce winds. The neutral wind attempts to move the ionization and hence influences the ionization density. The various nighttime wind effects at midlatitudes have been traced to the occurrence of what is called the 'midnight pressure bulge'. This phenomenon first reported by Nelson and Cogger[14] gives rise to the 'midnight descent' of the F-layer. A change in the direction of the meridional neutral wind has been identified as the cause of this midnight descent[16,17].

Studies on nighttime F-region vertical drifts have been made at some equatorial and midlatitude stations in the American longitudes using VHF backscatter and incoherent scatter radars. Not much work has been reported on the latitudinal dependence of these vertical movements. An attempt is made in the present study to examine the nighttime F-region height changes at equatorial, low and midlatitude stations in India and to compare these with the results obtained in the American sector.

2 Data and Analysis

Monthly averages of hourly $h'F$ (minimum virtual height for the lowest F-region stratification) values are taken for the period 1500-1600 hrs LT from published ionospheric data for the stations Kodaikanal (dip, 3.5°N), Hyderabad (dip, 21.5°N) and Ahmedabad (dip, 34°N) for different years between 1968 and 1978. Hourly rate of change of $h'F$ (in m/sec) is calculated to represent the F-layer vertical movement. Yearly average diurnal curves are plotted and shown in Figs 1-3 for Kodaikanal, Hyderabad and Ahmedabad respectively.

The method of determination of vertical speeds from the rate of change of virtual heights is one of the earliest, and gives a fair estimation of the layer movements at F-region heights at night.

3 Results

At Kodaikanal (a near-equatorial station), F-layer moves upwards slowly till around 1700 hrs and it

shows a rapid motion in between 1800 and 1900 hrs (Fig. 1). Around 1900 hrs an abrupt post-sunset upward-to-downward reversal of motion occurs. It is interesting to see that this reversal is very consistent in all the years of observation. A small downward movement is maintained throughout the night till a pre-sunrise reversal occurs. The behaviour is quite different at Ahmedabad (a midlatitude station). Here the maximum in upward motion is noticed between 2100 and 2200 hrs and an upward-to-downward reversal around midnight hours (Fig. 3).

The maximum upward motion occurring during 1800-1900 hrs at Kodaikanal and during 2100-2200 hrs at Ahmedabad seemed to be varying in magnitude in different months. Therefore, the value of the vertical speed in those hours for Kodaikanal and Ahmedabad for different months are plotted for different years and shown in Figs 4 and 5. A very prominent semi-annual oscillation can be seen in the vertical speed variation at Kodaikanal, with peaks in the equinoxes. At Ahmedabad there appears to be a broad maximum during summer months and a minimum during winter months.

At Hyderabad (a low midlatitude station), the nighttime F-layer movement shows a peculiar behaviour (Fig. 2). There appears to be a post-sunset upward-to-downward reversal around 1900 hrs. But the downward motion again becomes slightly upward for a short duration during pre-midnight hours.

Some results of earlier works[18-20] and of the present study pertaining to post-sunset/midnight F-region vertical drift reversal (upward-to-downward) at

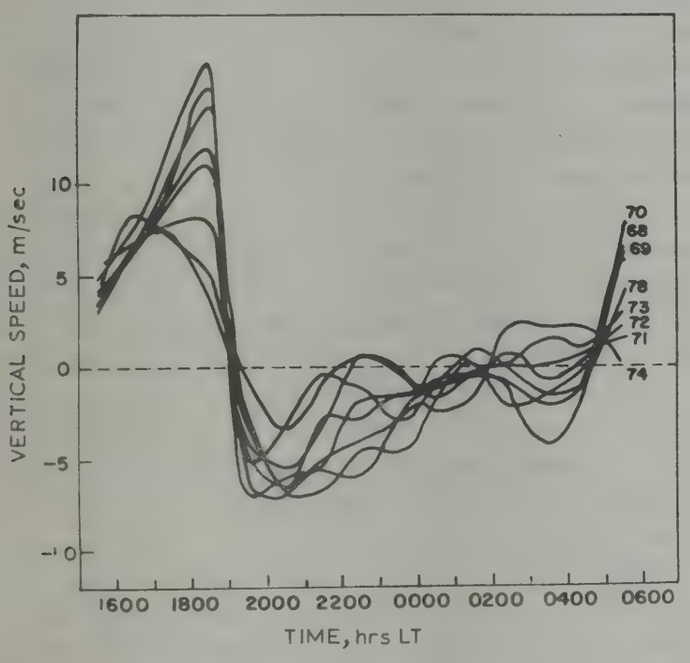

Fig. 1—Annual mean hourly rate of change of $h'F$ during 1500-0600 hrs LT for different years at Kodaikanal

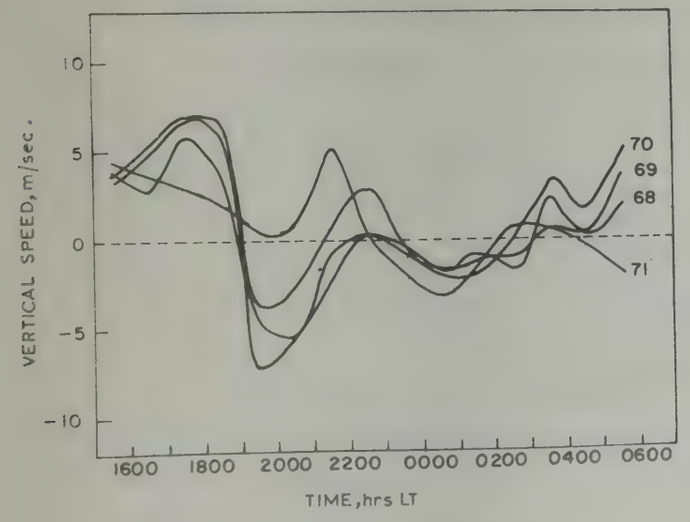

Fig. 2—Same as Fig. 1 but for Hyderabad

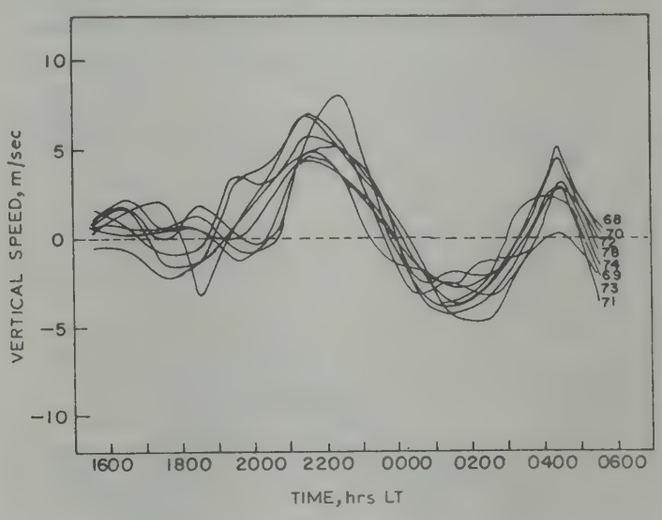

Fig. 3—Same as Fig. 1 but for Ahmedabad

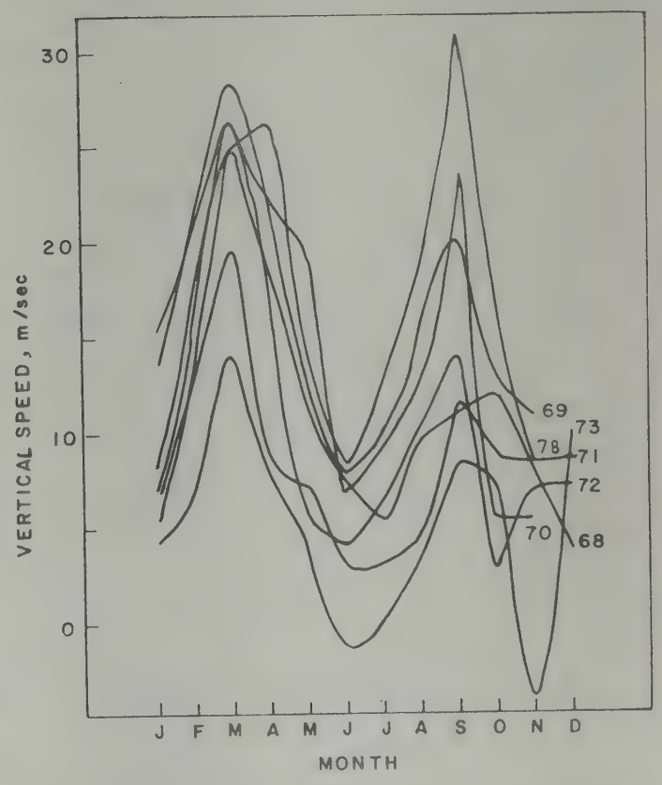

Fig. 4—Seasonal variation of post-sunset vertical drifts for different years at Kodaikanal

different Indian stations are given in Table 1 for comparison. It is seen that the time of occurrence of the upward-to-downward reversal increases from sunset time with increase in latitude away from the equator.

4 Discussion and Conclusions

The pattern of vertical movements as observed above at Kodaikanal are in accordance with the $\mathbf{E} \times \mathbf{B}$ drifts well known to be taking place at equatorial latitudes. One of the most striking discoveries of incoherent scatter observations of ionospheric motions has been the observation of vertical drifts at the equator which confirms the fountain theory of the equatorial anomaly. The F-region vertical drift observed at Jicamarca (dip, 2°S) has been interpreted as arising from $\mathbf{E} \times \mathbf{B}$ drifts caused by the east-west electric field associated with the equatorial electrojet

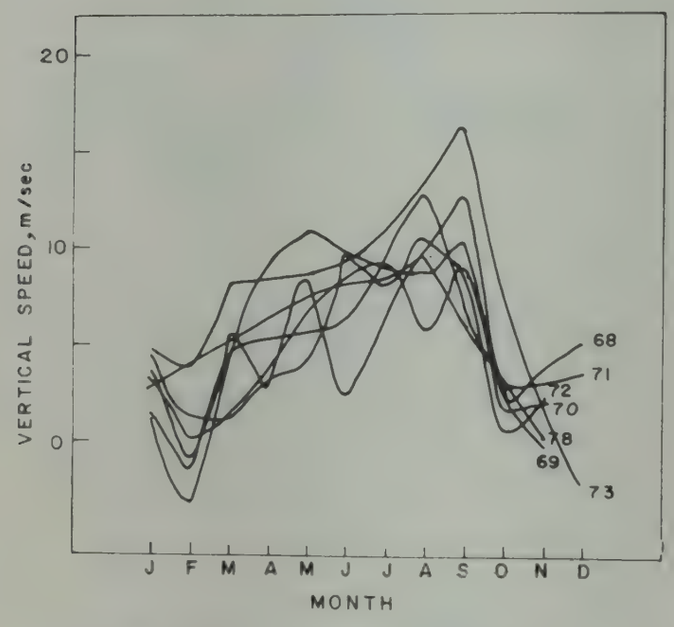

Fig. 5—Same as Fig. 4 but for Ahmedabad

and this hypothesis has been confirmed by several workers[7,21-23]. The sunset increase in the upward F-layer movement, the post-sunset reversal of motion and the nighttime slow downward movement observed at Kodaikanal seem to be arising out of these $\mathbf{E} \times \mathbf{B}$ drifts.

The midnight descent observed at Ahmedabad is interesting and a similar feature has been reported for some midlatitude stations in the American longitudes.

The general effect of the meridional neutral wind on the ionosphere away from the equator is to move the F-region ionization along the magnetic field lines. In the northern hemisphere, when the wind blows polewards, it tends to push the ionization downward; and when it blows equatorwards, it tends to push the ionization up along the magnetic field lines. Nighttime neutral wind studies by Behnke and Harper[16] at a midlatitude station (Arecibo) show that after initially strong equatorward winds, maximizing at about 2200 hrs, the winds decrease and blow polewards by midnight. This is attributed as the cause for the sudden midnight descent of F-layers at midlatitudes. The behaviour at Ahmedabad noticed in the present study seems to be consistent with the above observation.

The observed seasonal variation of the nighttime vertical drifts at Kodaikanal and Ahmedabad also confirms the importance of electric fields at the equatorial station and neutral winds at the midlatitude station. Woodman[7] summarized a large number of vertical drift measurements made at Jicamarca for different seasons and found that large vertical drifts occur during equinoxial months. Other results from Jicamarca data show rapid increase in h_{max} F2 after sunset during equinoxial months[10].

Application of the model wind theory at midlatitudes predicts stronger equatorward winds (upward vertical motion in the northern latitudes)

Table 1—Post-sunset/Midnight F-region Vertical Drift Reversal at Different Indian Stations

Station	Magnetic dip (geogr. lat.)	Upward-to-downward reversal time (hrs LT)	Measurement technique
Kodaikanal	3.5°N (10°14'N)	1900	Rate of change of $h'F$ (Present study)
Waltair	20°N (17°43'N)	1900 2330	Phase path[18]
		1900 0000 (Winter)	
		1830 2300 (Equinox)	Phase path[19]
		1930 2245 (Summer)	
Hyderabad	21.5°N (17°21'N)	1900 2200-0000	Rate of change of $h'F$ (Present study)
Ahmedabad	34°N (23°01'N)	2300-0000	Rate of change of $h'F$ (Present study)
Varanasi	(25°19'N)	0200	Phase path[20]

during summer nights[16]. Cho and Yeh[11] have shown that in summer, during sunset period, the meridional wind blows equatorwards and moves the F2-layer upward but in winter the wind becomes equatorward late in the post-sunset period. They also point out that the magnitude of the neutral wind (equatorwards) is greater in summer than in winter. Recently, Burnside *et al.*[17] have reported a similar result. At midlatitude stations during summer months an increase in N_mF2 is often observed near sunset and it was shown to be due to the equatorward wind at night[10]. The results of the present study are consistent with the above findings.

The time of occurrence of the upward-to-downward vertical drift reversal is observed to increase from sunset time with increase in latitude away from the equator (Table 1). But the causative mechanisms for the F-layer vertical motions seem to be different at different latitudes. Electrodynamic drifts control the F-layer motions at equatorial latitudes (Kodaikanal) and neutral winds play a dominant role at midlatitudes (Ahmedabad and Varanasi). At intermediate latitudes (Hyderabad and Waltair) nighttime F-layer vertical movements could be due to the combined and/or competing effects of $\mathbf{E} \times \mathbf{B}$ drifts and neutral winds.

References

1 Abur-Robb M F K, *Planet & Space Sci (GB)*, **17** (1969) 1269.

2 Krishnamurthy B V & Rao B R, *J Atmos & Terr Phys (GB)*, **25** (1963) 209.

3 Farley D T, Balsley B B, Woodman R F & Meclure J P, *J Geophys Res (USA)*, **75** (1970) 7199.

4 Rastogi R G & Woodman R F, *Ann Geophys (France)*, **34** (1978) 31.

5 Maeda H, *Proceedings of International Conference on Ionosphere, held in July* 1962 *at Imperial College, London Institute of Physics and the Physical Society, London*, 1963.

6 Matsushita S, *Radio Sci (USA)*, **4** (1969) 771.

7 Woodman R F, *J Geophys Res (USA)*, **75** (1970) 6249.

8 Rishbeth H, *J Atmos & Terr Phys (GB)*, **29** (1967) 225.

9 Kohl H, King J W & Eccles D, *J Atmos & Terr Phys (GB)*, **30** (1968) 1733.

10 Sterling D L, Hanson W B, Moffet R J & Baxter R G, *Radio Sci (USA)*, **4** (1969) 1005.

11 Cho H R & Yeh K C, *Radio Sci (USA)*, **5** (1970) 881.

12 Evans J V, Brockelman R C, Julian R F & Reid W A, *Radio Sci (USA)*, **5** (1970) 27.

13 Vasseur G, *J Atmos & Terr Phys (GB)*, **31** (1969) 397.

14 Nelson G J & Cogger L C, *J Atmos & Terr Phys (GB)*, **33** (1971) 1711.

15 Harper R M, *J Atmos & Terr Phys (GB)*, **35** (1973) 2023.

16 Behnke R A & Harper R M, *J Geophys Res (USA)*, **78** (1973) 8222.

17 Burnside R G, Herrero F A, Meriwether J W (Jr) & Walker J G C, *J Geophys Res (USA)*, **86** (1981) 5532.

18 Ernest Raj P, Srirama Rao M, Jogulu C & Rao B M, *Indian J Radio & Space Phys*, **9** (1980) 147.

19 Satyaramesh K, Srirama Rao M, Rao B M & Jogulu C, *Preprint Vol, National Space Science Symposium, Pune*, 1983, p.11.

20 Srivastava S K, Pradhan S M & Tantry B A P, *Ann Geophys (France)*, **26** (1970) 881.

21 Balsley B B & Woodman R F, *J Atmos & Terr Phys (GB)*, **31** (1969) 865.

22 Balsley B B, *J Geophys Res (USA)*, **74** (1969) 1213.

23 Balsley B B, *J Atmos & Terr Phys (GB)*, **35** (1973) 1035.

Indian Journal of Radio & Space Physics
Vol. 13, August 1984, pp. 116-118

Study of TEC & Equivalent Slab Thickness & Their Relationship with Ion Drifts & Ionospheric Temperatures

V K PANDEY, K K MAHAJAN, V C JAIN & R KOHLI
National Physical Laboratory, New Delhi 110012

Received 25 *June* 1984

The relationships of daytime total electron content and equivalent slab thickness with ion drifts and ionospheric electron temperature, respectively, have been examined. The data have been taken from the incoherent scatter radar measurements at Arecibo (lat., 18.3°N; long., 66.7°W) for the period Aug. 1974-May 1977. Some 800 profiles of electron density, electron temperature and ion drifts have been analyzed. The electron content is found to increase with increase in the vertical ion drift. There is, however, a time lag between the change in the ion drift velocity and the effect on electron content and this time lag varies from a few minutes to several hours, depending upon the height of the F-layer peak. The daytime equivalent slab thickness is seen to increase with the increase in electron temperature.

1 Introduction

Measurements of the electron content of the ionosphere have been made mostly by using the radio beacons on the low orbiting and geostationary satellites. An important result on the electron content has been its large variability from one day to the next and this could only be identified from the long continuous records obtained from the geostationary satellites[1-3] like Syncom-3, ATS-3 and ATS-6. While this variability, by and large, reflects changes in peak electron density, another important parameter which can cause this variability is the equivalent slab thickness, which is the ratio of electron content and peak electron concentration. Unfortunately, the radio beacons do not give information on any other parameter which controls the electron content and the slab thickness. It is now known from theory that the F-region electron content, in addition to the familiar loss and production mechanisms, is significantly controlled by the ion drifts. The incoherent scatter technique simultaneously measures the electron concentration, electron and ion temperatures, and ion drifts. In this paper we shall study the behaviour of electron content and equivalent slab thickness in relation to these simultaneously observed parameters by using the incoherent scatter measurements at Arecibo (18.3°N, 66.7°W).

2 Experimental Data

The incoherent scatter data used in the present analysis have been taken from radar measurements at Arecibo for the period Aug. 1974-May 1977. The measurements were made under the I9/I29 observation program of the Arecibo Ionospheric Observatory, as described by Harper and Ganguli[4].

The data have been obtained from the World Data Center A for Solar and Terrestrial Physics, Boulder, Colorado, USA. The electron and ion temperatures were deduced assuming a pure O^+ ionic composition[5] above 250 km. The Arecibo measurements gave (N/N_{max}) as a function of height. The peak electron density was read from an on-site ionosonde and thus the true electron density profile was obtained.

As the electron density profiles were available only up to an altitude of 500 km, we obtained the total electron content (TEC) during daytime (0800-1600 hrs), by performing the numerical integration of the electron density profile up to 500 km only. This procedure obviously results in underestimating the electron content. But as major contribution to the electron content comes from heights around the F2 peak, the underestimation may not be very significant since the contribution from heights above 500 km is perhaps not more than 15%.

As the incoherent scatter radar directly measures the normalized electron density profile (N/N_{max}), the integrated normalized profile gives the equivalent slab thickness directly and, therefore, the slab thickness is a more reliable parameter from the incoherent scatter radar measurements. The vertical ion drift velocity (V_z) and electron temperature (T_e) data have been taken for a height of 261 km to represent approximately the conditions around the height of F2 peak.

3 Variations of TEC and V_z

Fig. 1 shows the daytime variation of TEC and V_z for three days, one each during winter, equinox and summer seasons of the year 1976. The height of the peak electron concentration is also plotted in Fig. 1. As we know, the upward ion drift will take the ionospheric

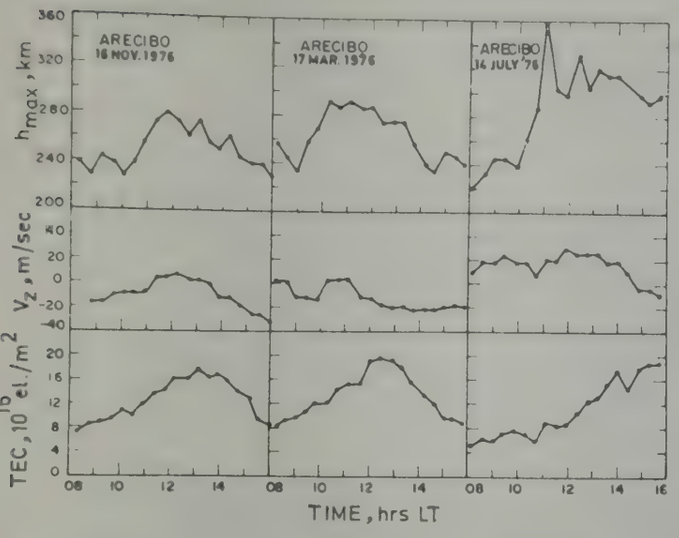

Fig. 1—Daytime variations of TEC, vertical component of ion drift velocity (V_z) at 261 km altitude and height of the peak electron density at Arecibo

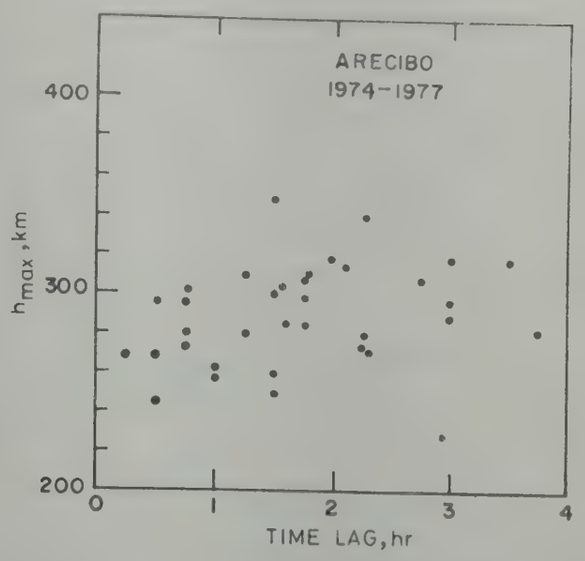

Fig. 2—Plot of the time lag between peaks of electron content and V_z as against h_{max}

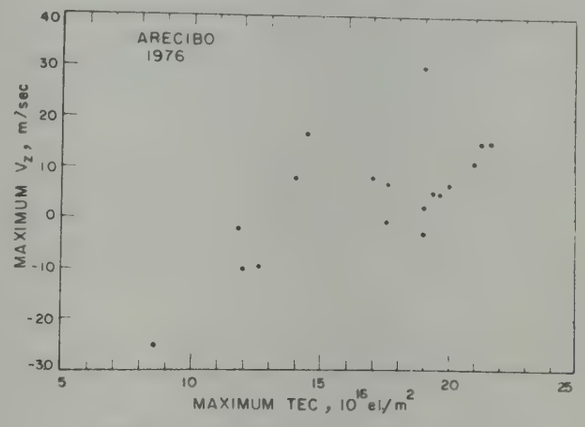

Fig. 3—Scatter plot of daytime maximum TEC and maximum V_z for all the days during 1976

F-region to higher heights to regions of lower electron loss rates, thus resulting in an increase in electron concentration (and TEC) during daytime. It can be noted that on all the 3 days the daytime electron content increases with increase in the vertical ion drift velocity and decreases with decreasing vertical ion drift velocity. There is, however, a time lag between the change in the ion drift velocity and its effect on TEC variation. This time lag is different for the three days and depends mainly on the height of peak electron density (h_{max}) as can be noted from the diagram where h_{max} is also plotted. During the winter day, when h_{max} was low, TEC variation responded rather fast to changes in V_z, i.e. the time delay between changes in V_z and corresponding changes in TEC was quite small (of the order of few minutes), as can be noted for the case of 16 Nov. 1976. The peak in V_z occurred around 1215 hrs and the peak in TEC around 1300 hrs, i.e. the time lag was about 45 min. On the day during equinox, when h_{max} was a little higher than the winter day, this time lag increased, as can be seen from the case of 17 Mar. 1976. The peak in V_z occurred around 1100 hrs and in TEC it occurred around 1230 hrs. On the day during summer when h_{max} was the highest, the time lag was maximum as can be seen for 14 July 1976 (Fig. 1). The peak in V_z occurred around noontime and the variation of TEC could not show the occurrence of clear peak, even at 1600 hrs. Further, to study the dependence of time lag (i.e. electron loss coefficient) on the height of peak electron density (h_{max}), we have examined all the data on electron density and V_z for the period Aug. 1974-May 1977. Diurnal plots of V_z and electron content were obtained for all days during this period for local times between 0800 and 1600 hrs. We then selected only those cases where diurnal peaks could be found both in V_z and electron content. The time lag between these two peaks were then plotted against the h_{max}, corresponding to the time of the V_z peak, as shown in Fig. 2. It is clear from the scatter plot that a positive correlation exists between h_{max} and time lag, thereby demonstrating that electron loss rates are high at lower heights and decrease with height.

It is difficult to study the relationship of TEC and V_z for long term variations, as one cannot unambiguously account for the changes in the response time due to changes in h_{max}, following the V_z changes. We have, however, attempted to study this correlation by plotting the maximum daytime values of TEC against maximum daytime values of V_z for the year 1976 as shown in Fig. 3. However, it was ascertained, that the time lag between the occurrence of peaks of these two parameters was consistent with the electron loss rate expected at h_{max}. There is a fair correlation between maximum TEC and maximum V_z during daytime, thus demonstrating the effect of ion drifts on TEC.

4 Variations of Slab Thickness and T_e

Fig. 4 shows the variation of daytime (0800-1600 hrs) slab thickness and electron temperature on 3 days,

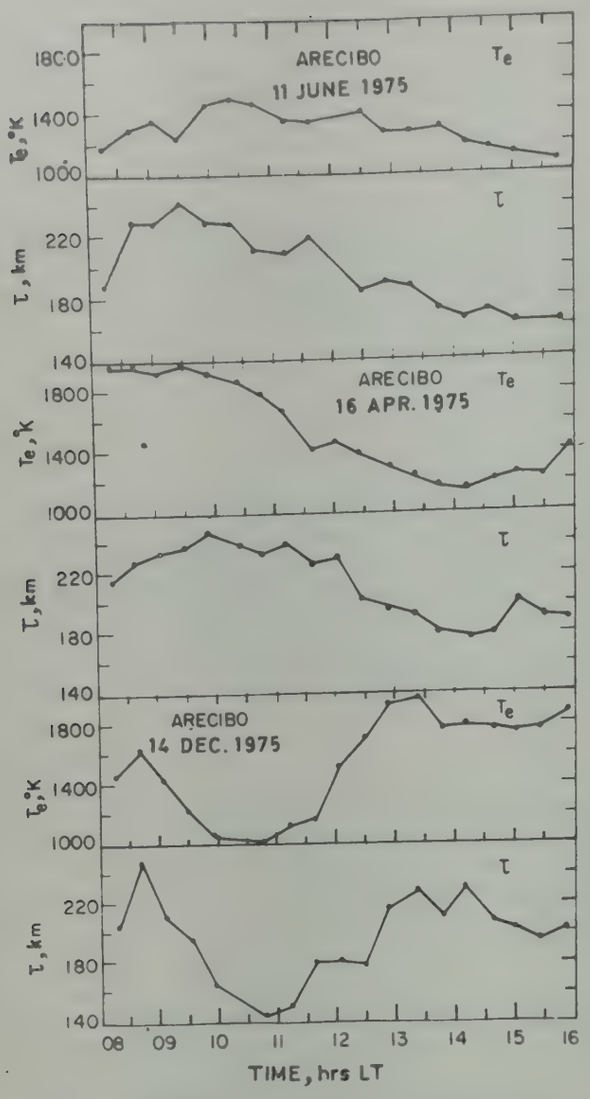

Fig. 4—Daytime variations of equivalent slab thickness and electron temperature at an altitude of 261 km on three days during 1975

one each in winter, equinox and summer during 1975. It can be noted that during all the seasons, changes in T_e are faithfully reflected in changes in slab thickness. On 14 December 1975, there are two peaks in T_e variation occurring around 0845 and 1400 hrs and the variation in slab thickness shows the occurrence of similar peaks, exactly at the same local time. The nature of variations in slab thickness and electron temperature is identical in equinox and summer seasons also.

Fig. 5 shows the scatter plot of equivalent slab thickness against electron temperature for noontime (1100-1300 hrs) for all the available days during 1975 and 1976. The temperature values were taken for a height of 261 km. From the scatter of points it is clearly noted that a fair positive correlation exists between

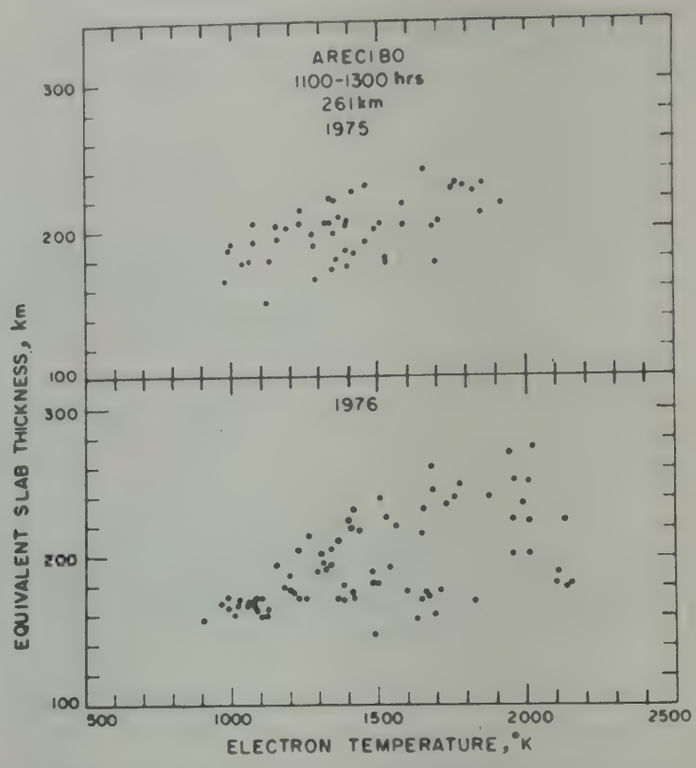

Fig. 5—A scatter plot of noontime electron temperature at an altitude of 261 km and equivalent slab thickness during 1975 and 1976

these two parameters. This correlation between slab thickness and T_e was reported by Mahajan *et al.*[6] from the earliest measurements at Arecibo.

Thus from the short term as well as long term variations of τ and T_e during daytime, it is seen that the slab thickness can be taken as an index of ionospheric electron temperature around the F2 peaks.

Acknowledgement

The authors are thankful to the Arecibo Ionosphere Observatory, Arecibo, Puerto Rico, USA, and the World Data Center A for Solar Terrestrial Physics, Boulder, Colorado, USA, for making available the I9/I29 data tapes for the period Aug. 1974-May 1977.

References

1 Garriot O K, Smith F L & Yuen P C, *Planet & Space Sci (GB)*, **13** (1965) 829.

2 Klobuchar J A & Allen R S, *Tech rep AFCRL-70-0403, Massachusetts, USA*, 1970.

3 Davies K, Fritz R B & Gray T B, *J Geophys Res (USA)*, **81** (1976) 2825.

4 Harper R & Ganguli S, *Arecibo Observatory Document, Arecibo, Puerto Rico, USA*, 1977.

5 Torr M R & Harper R, *Radio Sci (USA)*, **12** (1977) 461.

6 Mahajan K K, Rao P B & Prasad S S, *J Geophys Res (USA)*, **73** (1968) 2477.

Indian Journal of Radio & Space Physics
Vol. 13, August 1984, pp. 119-124

Diurnal & Seasonal Variation of Frequency Dependence of Ionospheric Absorption at a Tropical Latitude

D B PATEL & K M KOTADIA
Physics Department, Gujarat University, Ahmedabad 380 009

Received 2 *March* 1984

Multifrequency ionospheric Al-absorption data obtained at Ahmedabad (23° N, 72.6° E, mag. dip 34° N) are analyzed to study the frequency dependence of absorption for low and high solar activity epochs, and also for low and moderately high solar activity years (1976 and 1978). The exponent m in the inverse frequency dependence of measured absorption is determined for practical purposes. The diurnal variation of the index m for different months and its seasonal variation at a fixed solar zenith angle (SZA) are studied for total absorption (L_{total}) as well as for its non-deviative (L_{nd}) part. It is found that L_{total} does not obey the inverse frequency square law. During sunspot minimum, m is found to vary with time of the day showing maximum (annual average = 0.71) around noon and falling towards morning and evening hours, whereas for sunspot number $R_z = 100$, it shows the opposite trend showing minimum (average value = 0.60) around noon and increasing towards morning and evening hours. In the case of non-deviative (L_{nd}) absorption, the index m in 1976 and 1978 behaves in a manner similar to that of L_{total} for $R_z = 00$ and 100, but m for L_{nd} has higher values and range of variation, the values being clustered around the theoretical value 2 near noon, in the spring months of 1976 and for most part of the day in August 1978. These results suggest that the higher value of m on the average for L_{total} during increased solar activity is due to major contribution of non-deviative absorption and only small contribution of deviative absorption to the total absorption during high solar activity. It is also verified that the value of the proportionality constant A in the assumed frequency dependence law of total absorption changes with time or SZA corresponding to the changes in the value of m.

1 Introduction

The non-deviative absorption of ordinary radiowave measured on different frequencies at the same solar zenith angle (SZA, χ) should, according to classical magnetoionic theory of radio wave propagation in the ionosphere, vary inversely as the square of the effective frequency $(f+f_L)$ when $\nu \ll \omega$. This can be expressed by the relation $L = A/(f+f_L)^2$ where A is a constant depending on the electron density N and collision frequency ν, f_L is long longitudinal component of electron gyromagnetic frequency and $\omega = 2\pi f$ is the observing radio frequency. When f is near the critical frequency of a layer, and where ν and ω are comparable, the inverse frequency square law fails. Appleton and Piggott[1] demonstrated from the measurements at Slough, that the increase in absorption near the critical frequency of E and Fl layers was due to appreciable deviative absorption. To distinguish between the deviative and non-deviative absorption, Bibl *et al.*[2] and Beynon and Davies[3] gave different formulae which included a second term to account for the deviative absorption involving a function of f/f_0E, f_0E being the ordinary wave critical frequency of the E-layer. Reference is also made to the work of George[4], later extended by Samuel and Bradly[5] who proposed the so called A-figure which also involves a function of f/f_0E. Some workers[6-8] have tried to prove the inverse frequency square law of absorption at midlatitudes, but with not much success. Near the equator, the absorption obeys nearly the inverse frequency law[9-11] ($m = 1$). At low latitudes[12-15], the value of m was found to vary with time and season from 1.1 to 2.4 depending on the stage of solar activity.

In this paper, use is made of the Al ionospheric absorption data obtained at a tropical latitude station, Ahmedabad (23°N, 72.6°E, mag. dip. 34°N) on three frequencies, viz. 1.8, 2.2 and 2.5 MHz from 1972 to 1980. The frequency index m has been calculated for total, i.e. measured absorption at different times of the day in different months for the two epochs of solar activity (viz. $R_z = 00$, and 100) for its usefulness in solar-terrestrial prediction and practical communication. The same is done for non-deviative (L_{nd}) absorption for the years 1976 and 1978 representing low and moderately high solar activity, for comparison with the total absorption during the two epochs, viz. $R_z = 00$ and 100 and to understand the physics of the absorbing region. Seasonal variation of the index m is also shown at fixed cos χ for the two epochs of solar activity.

2 Method of Analysis

The variation of ionospheric absorption with sunspot number at different times (8 to 17 hrs) of the day for each month was calculated by taking the

respective monthly median values of total absorption on three frequencies for the years 1972-80. The method of least-square fitting was used to establish the linear relation between L_{dB} and sunspot number R_z in the form $L_{dB}=a(1+bR_z)$, from which monthwise hourly values of absorption at $R_z=00$ and $R_z=100$ were calculated.

A rough estimate of deviative absorption was made by using Jaeger's[16] formula which includes cos χ and a function of f/f_0E, taking appropriate values of the parameters therein. Knowing L_d, non-deviative absorption L_{nd} was separated from the total for 1976 and 1978. The frequency dependence is then investigated for L_{nd} also in a manner similar to that used for the observed total absorption. The dependence power m is evaluated from the plots of absorption and frequency on a log-log graph paper, line fitting done by computer for three points. There is some controversy about the reliability of Jaeger's formula, but we have found that L_d calculated by using it agrees fairly well with that found from the reflections from the low-type blanketing Es-layer occurring at our tropical place, Ahmedabad. Also, the changes in the thus determined L_{nd} and those in the A-figure of George[4] during a solar eclipse are found to be nearly the same from the work of Patel *et al.*[7] Solar cycle variation of L_{nd} at different times for each month has not been attempted, and so we have shown it for 1976 and 1978 ($\bar{R}_z=10$ and 93, respectively), years fairly comparable with $R_z=00$ and $R_z=100$ stages of the solar cycle.

3 Diurnal Variation of Index m for Total Observed Absorption

In Fig. 1, power or index m of the inverse frequency dependence of absorption is plotted against time of the day for each month for the solar epochs $R_z=00$ and $R_z=100$. It is clearly seen that the total absorption does not obey inverse frequency square law at either stage of the solar cycle. At SS_{min} (sunspot minimum), index m is maximum near noon (annual average 0.71) and decreases towards morning and evening hours around mean value of 0.5 in agreement with results of Waltair[14] for the period June 1961-Sep. 1962, ($\bar{R}_z=46$) except in the equinoctial months, viz. April and September when m has a shallow dip around noon and somewhat higher values in the forenoon and afternoon. But it should be noted that m in April is appreciably larger than in all other months, with a whole day mean value of 1.4. It is interesting to see that the shape of the diurnal variation of m at the stage $R_z=100$ reverses from that when $R_z=00$, i.e. m is minimum near noon with annual average of 0.60 and increasing towards morning and evening hours to a mean value around 0.8 with the exception of October, November and

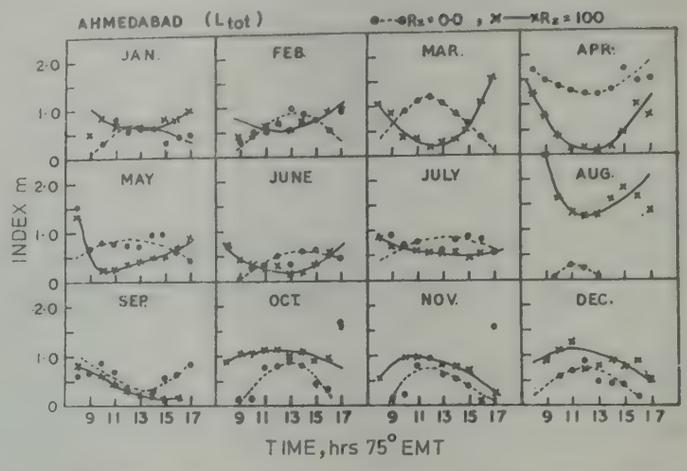

Fig. 1—Diurnal variation of the exponent m in the inverse frequency dependence of observed total ionospheric absorption in different months for $R_z=00$ and $R_z=100$ epochs (Date for August were incomplete for $R_z=00$)

December when it has a similar trend as during SS_{min} in addition, the level of m is raised up. The diurnal variation of m during midsummer months of SS_{min} is almost flat which means to indicate a condition of transition for it to change over to the type of the diurnal variation observed during high solar activity. There is some seasonal asymmetry in the diurnal variation, the maximum or minimum as the case may be occurring earlier in time during winter months and later in summer months in contrast to the diurnal maximum of observed absorption (later in winter and earlier in summer). The nature of diurnal variation of m at Ahmedabad agrees with that at a midlatitude station Kokubunji[8] and a low latitude station Waltair[18] for high solar activity period.

A much clearer picture of the diurnal variation of m for L_{total} is brought out by considering its averages over three seasons, viz. winter and summer solstices, equinoxes, and over the whole year. This is shown in Fig. 2. It is seen that the irregular scatter seen in the monthly diurnal variation of m disappears in the mean values and the reversal in its nature from low activity-type to high activity-type [Fig. 2(a)] is evident. The summer of low solar activity and winter of high solar activity appear to be transition stages for such reversal in the shape of diurnal variation of m because of the small ranges. The whole-day annual mean value of m during high solar activity is larger ($m=0.74$) than that during low solar activity ($m=0.55$). To sum up these features, Fig. 3 is drawn to show the variation of annual average observed absorption at 09, 12 and 15 hrs with effective frequency for $R_z=0$ and $R_z=100$ stages of solar activity. It may be noticed that the slope m is larger at 12 hrs than at forenoon and afternoon hrs for $R_z=0$ case, while it is smaller at 12 hrs than at the other two periods for $R_z=100$ case, the latter giving larger values of m on the whole. Another interesting

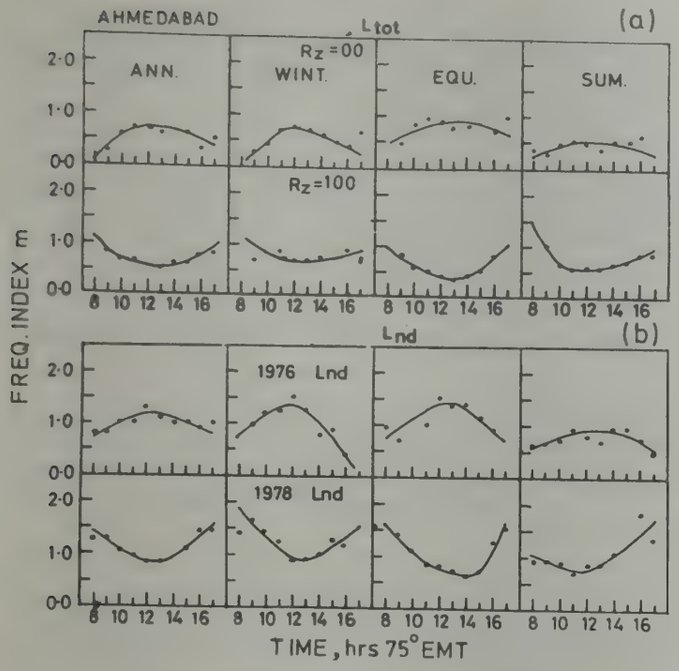

Fig. 2—(a) Mean diurnal variation of the exponent m for total absorption during three seasons and over the whole year for $R_z = 0$ and $R_z = 100$; (b) Same as above, but for non-deviative absorption during 1976 and 1978

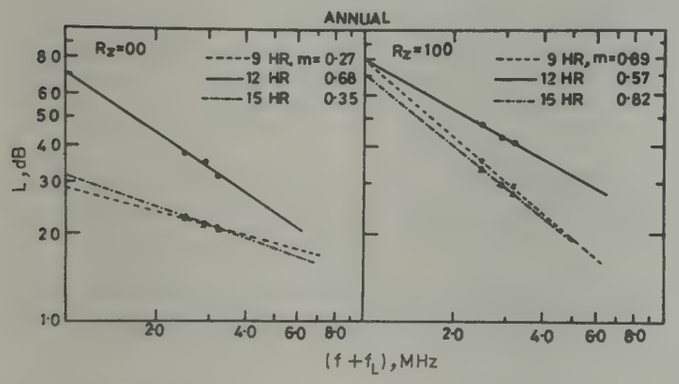

Fig. 3—Variation of annual average observed absorption with effective frequency at 09, 12 and 15 hrs for $R_z = 0$ and $R_z = 100$ (Note the reversed order in the values of m in its diurnal variation and the changes in the intercept on the vertical axis, i.e the proportionality constant A during low and high solar activity periods.)

point is that the intercept on L_{dB} axis, i.e. the constant of proportionality A also varies with time, it being much larger near noon than that at 09 and 15 hrs during low solar activity, but during high solar activity in spite of high values and larger range of variation of m, the constant A does not change much and remains at high level, around 70 to 80 dB(MHz)^m. Thus with the change in SZA, both m and A also vary, the variation in A during high solar activity being small. Later, we shall show how A depends on cos χ.

4 Diurnal Variation of m for Non-deviative Absorption (L_{nd})

In order to throw some more light on the result of changing values of m for L_{total} and opposite natures of its diurnal variation in low and high solar activity

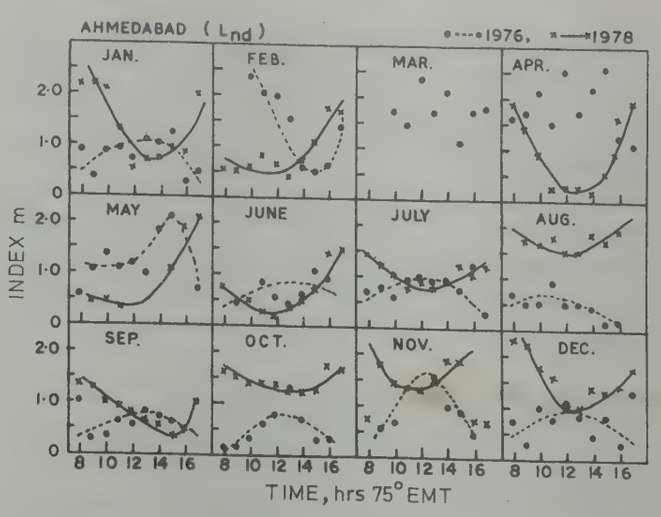

Fig. 4—Diurnal variation of the exponent m in the frequency dependence of non-deviative absorption during the years of low and moderately high solar activity, viz. 1976 and 1978

periods, an attempt is made to separate the deviative absorption (L_d) occurring in the E-layer from the total observed absorption and see if the remaining non-deviative absorption (L_{nd}) mostly occurring in the D-region of the ionosphere gives the theoretically expected value 2 for m in the frequency dependence law. The method for finding approximate value of L_d was described in Sec. 2. The values of m calculated for L_{total} in the years 1976 and 1978 were practically the same as those for the solar activity stages $R_z = 0$ and $R_z = 100$ as expected. Fig. 4 and Fig. 2(b) show the diurnal variation of m for each month separately and for averages over each season (and the whole year) respectively for the above stated two years. The most distinctive point revealed from the comparison of the diurnal variations of m for L_{total} and L_{nd} is a significant increase of the value of m for L_{nd} over that for L_{total}, a result also found by Ramanamurty and Rao[14] at Waltair (17.7°N, 83.3°E, mag. dip 21.5°N). Not only that, the range of diurnal variation of m for L_{nd} is also larger than that for L_{total}, but the common feature of reversal in the nature of diurnal variation of m for the two in each month and season with increase in solar activity is clearly noticeable, though at the increased level of m for L_{nd}. The diurnal variation of m for D-region absorption at Udaipur[13] (24.6°N, 73.7°E) obtained during low solar activity (1976-77) goes against the results for L_{nd} at Ahmedabad. There are also indications of m for L_{nd} approaching the theoretical value 2 more often. Inverse frequency square law seems to be realized in the months February, March, April and May during 10-15 hrs time-interval in 1976, and during forenoon and afternoon hours in 1978 except during forenoon hours in February, May and June. In some months, for example March and April 1976, the values of m are so much scattered around 2 that it is difficult to draw a

smooth curve through them although it has a tendency to fall at higher SZA near morning and evening hours. In substance, L_d taken together with L_{nd}, i.e. L_{total} brings down the value of m in contrast to that obtained for L_{nd} alone. Thus superposition of deviative absorption on the non-deviative absorption seems to be the reason for the total absorption not obeying the inverse frequency square law, leaving aside the constancy of A in it.

5 Seasonal Variation of m at Fixed SZA

From the diurnal variations of the index m in different months for low and high solar activities shown in Sections 3 and 4, it could be seen that the value of m changes appreciably, rather irregularly, at a given hour. One reason for such irregularity could be that the SZA does not remain at same value in different months at a given time, and this affects the contributions of L_d and L_{nd} to the total absorption and hence its frequency dependence also. To study purely seasonal variation, SZA and R_z should be taken as fixed parameters. In Fig. 5 are shown the seasonal variations of the index m for L_{total} and L_{nd} at $\cos\chi = 0.60$ during two epochs of solar activity. In the case of L_{total}, the value of m during most part of the year remains at around 0.5 with a peak value of 1.5 in April of SS_{min}, the annual average coming to 0.71. At $R_z = 100$, the value of m for L_{total} during most part of the year lies around 0.75 to 0.80 with a peak value of 2.1 in August, giving annual average 1.03; so the equinoctial peak of m shifts to late-summer (or monsoon) month and the value on the average increases with increase in solar activity. Irregular month-to-month changes in the value of m also smooth out by taking constant $\cos\chi$. In the case of L_{nd}, the trend of seasonal variation of m is almost similar to that found for L_{total} but now m is around 1.4 in the first half of the year and 0.5 for the other half as against 0.5 during most part of the year for L_{total} during SS_{min}, the annual average of m for L_{nd} coming to 1.21 as compared to 0.71 for L_{total}. During 1978 of moderately high solar activity ($\bar{R}_z = 93$), the value of m remains above 1.0 for most part of the year,

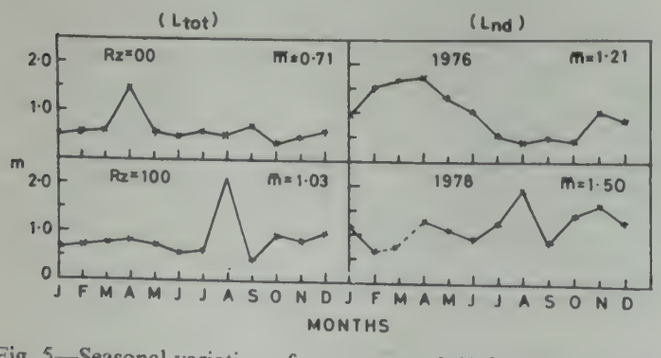

Fig. 5—Seasonal variation of m at $\cos\chi = 0.60$ for observed total absorption and calculated non-deviative absorption for low and high solar activity periods

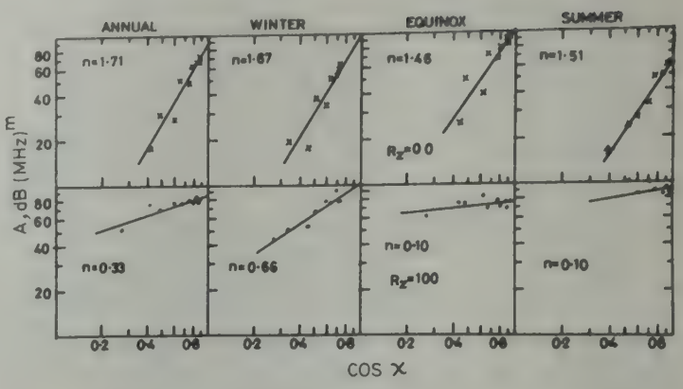

Fig. 6—Variation with $\cos\chi$ of the proportionality constant A in the frequency dependence law for total absorption (The slope gives the value of index n of $\cos\chi$ at $R_z = 0$ and $R_z = 100$ in different seasons and average for the whole year.)

Table 1—Values of Constant A_0 and Index n of $\cos\chi$ for Diurnal Variation of A at $R_z = 00$ and $R_z = 100$ Epochs

Season	A_0 dB(MHz)^m		n	
	$R_z = 0$	$R_z = 100$	$R_z = 0$	$R_z = 100$
Winter	96.9	101.1	1.67	0.66
Equinoxes	103.7	76.4	1.46	0.10
Summer	63.02	92.0	1.51	0.10
Annual	(87.26)	(85.69)	(1.71)	(0.33)

giving annual average 1.5 as compared to 1.03 for L_{total}. It, therefore, appears that the contribution of L_{nd} on the three frequencies is large in spring months of low solar activity and in late summer and autumn of high solar activity, but in either case it is definitely greater than the value of m for L_{total}.

6 Conclusions and Discussion

(i) During low solar activity, the exponent m of effective frequency in the inverse frequency dependence of the total observed absorption is found to be maximum at noon and decreasing towards morning and evening hours except in the month of April but it is far below the value 2. With the decrease in m, the constant of proportionality A also decreases. Fig. 6 shows variation of A with $\cos\chi$. It is evident that A for $\cos\chi = 1$ during low solar activity remains at about 85 and it varies from 20 to 80 in different seasons during the course of a day, it being at low level of 10 to 60, giving annual average range 15-70 dB (MHz)^m leaving the extrapolated value of A_0. The equation for L_{dB} at $R_z = 0$ can be written as

$$L_{dB} = \frac{A_0 \cos^n\chi}{(f + f_L)^m}$$

and the values of A_0 and n are given in Table 1.

With increase in SZA, f_0E decreases, height of reflection increases where $\nu \ll \omega$; so the deviative

absorption increases by different amounts, and the net effect on the frequency dependence is the decrease in the value of m at higher SZA. The deviative absorption was shown to vary roughly from 20% at noon to about 40% of total at 08 and 17 hrs during low solar activity by Kotadia *et al.*[19]. Change of A with m means change in $\int Nv\,dh$ or $N(h)$ profile if the collision frequency $\nu(h)$ profile is assumed not to vary with time. Here $N(h)$ stands for electron density distribution with height.

(ii) During high solar activity, the curve of diurnal variation of m reverses in shape from that found for low solar activity; however, the values of m are on the whole larger during high solar activity, but still smaller than two. Such a behaviour is expected when the contribution of deviative absorption is comparatively smaller than that of non-deviative absorption to the total. Also, the descending of the absorbing and reflecting layers with increased electron density and ν becoming comparable with $(\omega+\omega_L)$ might cause the diurnal variation of m with minimum at noon and increasing towards morning and evening hours. With increase in m, A also increases though the variation in A is not so much as that found during low solar activity (See Figs 3 and 6). It changes hardly by 10 in summer and equinoxes while by 50 in winter, the annual average range being 50-85 dB $(\text{MHz})^m$. Under these conditions, the equation for absorption has to be written as

$$L_{dB}=\frac{A'_0\cos^n\chi}{(f+f_L)^m}$$

in which A'_0 stands for $A_0(1+bR_z)$ taking care of m, n and increased $N(h)$, and b is the factor by which the absorption increases with sunspot number relative to its value at $R_z=0$. Appropriate values of A_0, A'_0, n and m have to be inserted in the above formula for prediction of total absorption on different frequencies at a given time/SZA and R_z. For convenience of the user engaged in radio communication, values of m (Fig. 2) are given in Table 2.

(iii) In some months, m is found to remain nearly constant or it changes very little with time, e.g in summer of low solar activity and winter of high solar activity. Such a condition marks the transition stage for the low solar activity-type to the high solar activity-type of diurnal variation of m, and during such transition period, the deviative and non-deviative components of total absorption are probably maintained in the same proportion. There are cases when m falls to very low values, as low as 0.25 or still lower, during most of the months of low solar activity at high SZA and around noontime in spring and summer months of high solar activity. Explanations for such low values of m may be given as in items (i) and (ii) above referring to $\int Nv\,dh$ and ν becoming comparable with $(\omega+\omega_L)$. Total absorption calculated using the N-h profiles[20,21] constructed for different SZA and for low and high solar activity periods substantiates the results presented here in the diurnal variation of m for L_{total}.

(iv) The diurnal variation of m for non-deviative absorption (L_{nd}) behaves in the same manner as that for the total absorption (L_{total}), but with a major difference in the values of m for L_{nd} which are larger than for L_{total}. This gives a positive evidence for L_{total} not obeying the inverse frequency square law since it contains L_d

Table 2—Mean Exponent m in the Frequency Dependence of Total Observed Al Absorption at Different SZA and in Different Seasons for $R_z=00$ and $R_z=100$ Epochs

Season												Whole day mean of m
						(i) $R_z=0$ Epoch						
Winter	$\cos\chi$:	0.27	0.46	0.60	0.70	0.74	0.72	0.64	0.51	0.34	0.14	
	m:	—	0.23	0.40	0.69	0.75	0.67	0.60	0.46	0.36	0.65	0.53
Summer	$\cos\chi$:	0.53	0.71	0.86	0.95	0.995	0.98	0.9	0.77	0.60	0.39	
	m:	0.37	0.29	0.47	0.52	0.50	0.39	0.51	0.52	0.63	—	0.46
Equinox	$\cos\chi$:	0.44	0.63	0.78	0.88	0.92	0.89	0.81	0.67	0.48	0.27	
	m:		0.48	0.82	0.95	0.87	0.77	0.80	0.84	0.69	0.96	0.80
Annual mean	$\cos\chi$:	0.41	0.60	0.75	0.84	0.88	0.86	0.78	0.65	0.48	0.27	
	m:	0.08	0.26	0.56	0.72	0.71	0.61	0.64	0.61	0.30	0.51	0.55
						(ii) $R_z=100$ Epoch						
Winter	$\cos\chi$:	0.27	0.46	0.60	0.70	0.74	0.72	0.64	0.51	0.34	0.14	
	m:	0.54	0.70	0.84	0.89	0.69	0.69	0.75	0.75	0.91	0.68	0.74
Summer	$\cos\chi$:	0.53	0.71	0.86	0.95	0.995	0.98	0.90	0.77	0.60	0.39	
	m:	1.50	1.03	0.67	0.60	0.62	0.60	0.69	0.77	0.85	0.86	0.82
Equinox	$\cos\chi$:	0.44	0.63	0.78	0.88	0.92	0.89	0.81	0.67	0.48	0.27	
	m:	0.98	0.85	0.60	0.51	0.44	0.37	0.44	0.53	0.80	1.01	0.65
Annual mean	$\cos\chi$:	0.41	0.60	0.75	0.84	0.88	0.86	0.78	0.65	0.48	0.27	
	m:	1.16	0.86	0.70	0.66	0.58	0.55	0.63	0.61	0.78	0.82	0.74

besides L_{nd}. The inverse frequency square law is nearly realized at most times in the case of L_{nd} and this is also the reason why m values for L_{total} during high solar activity are effectively larger than during low solar activity. The function $\varphi(f/f_0E)$ joined up with the product of L_{total} and $(f+f_L)^2$ also alters the value of the A-figure proposed by George[4] according to the conditions prevailing in the D and E region ionization. In the A-figure m is taken as 2 according to the theoretical expression for L_{nd}.

(v) The seasonal variation of m for L_{total} and L_{nd} at constant SZA and R_z shows higher values in spring months during low solar activity, but it is so in late summer/autumn months during high solar activity. The annual averages of m for L_{total} at $\cos\chi=0.6$ are 0.71 for $R_z=0$ and 1.03 for $R_z=100$ epochs. Corresponding average values of m for L_{nd} are 1.21 and 1.5.

(vi) Finally, the ionospheric absorption of HF radio waves on different frequencies for any time/SZA, season and stage of sunspot cycle can be easily predicted with the help of results obtained in this paper for the exponent m and constant A_0, and the values of a and b (not given here) in the equation $L_{dB}=a(1+bR_z)$ for different times and months. Mean values of a and b for $\cos\chi=1$ and $\cos\chi=0.6$ for Ahmedabad were reported earlier[22].

Acknowledgement

The authors are grateful to the Council of Scientific and Industrial Research, New Delhi, and the University Grants Commission, New Delhi, for financial support in the research schemes. Thanks are also due to Dr K G Jani for his valuable assistance in the smooth functioning of the experimental set-up.

References

1 Appleton E V & Piggott W R, *J Atmos & Terr Phys (GB)*, **5** (1954) 141.
2 Bibl K, Paul A & Rawer K, *J Atmos & Terr Phys (GB)*, **23** (1962) 244.
3 Beynon W J G & Davies K, *Physics of ionosphere* (Physical Society, London), 1955, 40.
4 George P L, *J Atmos & Terr Phys (GB)*, **33** (1971) 1893.
5 Samuel J C & Bradley P A, *J Atmos & Terr Phys (GB)*, **37** (1975) 131.
6 Davies K & Hagg E L, *J Atmos & Terr Phys (GB)*, **6** (1955) 18.
7 Whitehead J D, *J Atmos & Terr Phys (GB)*, **10** (1957) 12.
8 Yasuda J, *J Atmos Res Labs (Japan)*, **10** (1963) 213.
9 Skinner N J & Wright R W, *J Atmos & Terr Phys (GB)*, **9** (1956) 103.
10 Gnanalingam S, *Proceedings of the third international symposium on equatorial aeronomy, Physical Research Laboratory, Ahmedabad*, 1969, 47.
11 Parameswaran K & Krishnamurthy B V, *J Atmos & Terr Phys (GB)*, **40** (1978) 1211.
12 Rao M K, Mazumdar S C & Mitra S N, *J Atmos & Terr Phys (GB)*, **24** (1962) 245.
13 Vijayavergia S K & Rai R K, *Indian J Radio & Space Phys*, **8** (1979) 366.
14 Ramanamurty Y V & Rao B R, *J Atmos & Terr Phys (GB)*, **26** (1964) 849.
15 Kotadia K M, Gupta A & Kotak R M, *Proceedings of the workshop on solar terrestrial predictions, Vol IV, Sect* 03 *NOAA, Boulder, USA*, 1980, 20.
16 Jaeger J C, *Proc Phys Soc (GB)*, **59** (1947) 87.
17 Patel D B, *Ph D thesis*, Gujarat University, Ahmedabad, 1984.
18 Chandrasekhar R, Victor P, Indiradevi D, Rao D N M, Somayaji T S N & Ramana K V V, *Indian J Radio & Space Phys*, **12** (1983) 43.
19 Kotadia K M, Chhipa G M & Taubenheim J, *Indian J Radio & Space Phys*, **6** (1977) 1.
20 Gupta A & Kotadia K M, *J Geophys (Germany)*, **46** (1979) 23.
21 Datta G, Pradhan S N & Kotadia K M, *Advances in Space Res (GB)*, **2** (1983) 209.
22 Kotadia K M, Datta G & Chhipa G M, *Indian J Radio & Space Phys*, **10** (1981) 171.

Indian Journal of Radio & Space Physics
Vol. 13, August 1984, pp. 125-128

Radiation Field Patterns of a Microstrip Slot Antenna in an Ionized Medium

N K GUJAR & R K GUPTA
Microwave Laboratory, Malaviya Regional Engineering College, Jaipur 302017

Received 30 *May* 1983; *accepted in final form* 2 *March* 1984

Expressions for the electromagnetic and the electroacoustic field components of a microstrip slot antenna radiating in an ionized medium are obtained. The slot antenna is assumed to be equivalent to a magnetic dipole with a prescribed magnetic current distribution. It is concluded that the field patterns of the slot are greatly affected by the presence of the ionized medium.

1 Introduction

Microstrip antennas have proved their superiority as low drag, low profile and light weight antenna. These are being increasingly used on space shuttles[1], high speed, high flying aircrafts and satellites[2] in the frequency band of 1 to 10 GHz. The presence of ionized medium encountered during the passage of the above high flying space vehicles will modify the properties of these antennas.

It has been conclusively proved that the presence of an ionized medium modifies the properties of antennas[3,4]. An antenna immersed in a warm isotropic ionized medium (plasma) generates electroacoustic wave in addition to the usual electromagnetic wave. In this paper, study is made about the effect of plasma on microstrip slot antenna using a well established linearized hydrodynamic theory and vector wave function technique. In our study, the motion of ions is neglected. Other assumptions are similar to those of Gupta and Freeston[4]. It is assumed that the antenna is immersed in homogeneous unbounded isotropic plasma of uniform density.

2 Theoretical Expression for the Field Patterns

The basic microstrip radiator following Derneryd[5] is shown in Fig. 1. The energy is radiated from the two slot antennas as indicated by the dotted lines.

The geometry of one of the slot antennas is shown in Fig. 2. We follow transmission line model for derivation of equations for field patterns.

The tangential electric field in the slot aperture is assumed as[6]

$$E_a = \hat{X} E_0 \cos\left(\frac{\pi y}{2b}\right), \quad |x| \le a, \quad |y| \le b \qquad \ldots (1)$$

This is equivalent to a magnetic dipole with magnetic current, viz.

$$I = -4aE_0 \cos\left(\frac{\pi y}{2b}\right)\hat{y}, \qquad |y| \le b \qquad \ldots (2)$$

Using Maxwell's equations and the linearized continuity and field equations for the ionized medium[7], the value of vector field $\mathbf{A}_y$ and scalar potential Φ are obtained as

$$\mathbf{A}_y = \frac{4\mu_0 a E_0}{rb} \exp\{j(wt - \beta_e r)\}[M_1](\sin\theta \sin\varphi \hat{r} + \cos\theta \sin\varphi \hat{\theta} + \cos\varphi \hat{\varphi}) \qquad \ldots (3)$$

and

$$\Phi = \frac{4\mu_0 a E_0 w}{rb\beta_e} \sin\theta \sin\varphi [M_1] \qquad \ldots (4)$$

where

$$[M_1] = \left[\frac{\sin(\beta_e a \sin\theta\cos\varphi)\cos(\beta_e b \sin\theta \sin\varphi)}{\beta_e \sin\theta\cos\varphi\{(\beta_e \sin\theta\sin\varphi)^2 - (\pi/2b)^2\}} \times \cos\{\beta_e (1/2)\cos\theta\}\right] \qquad \ldots (5)$$

The far zone electric field in the ionized medium is given by Stratton[8]

$$\mathbf{E}_e = -\nabla\varphi - jw\mathbf{A} \qquad \ldots (6)$$

Substituting the value from Eqs (3) and (4) in Eq. (6) the far zone electric field is obtained as

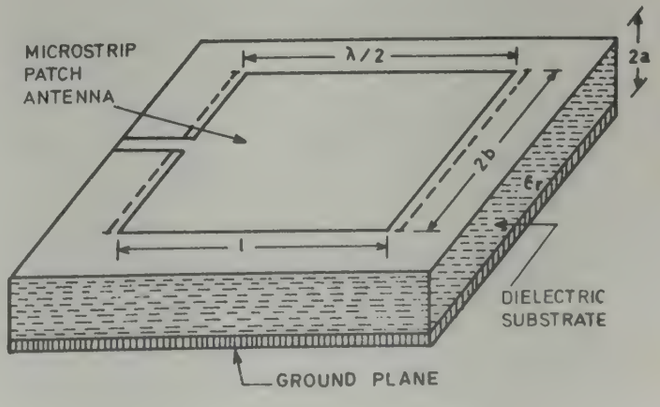

Fig. 1—Basic microstrip radiator

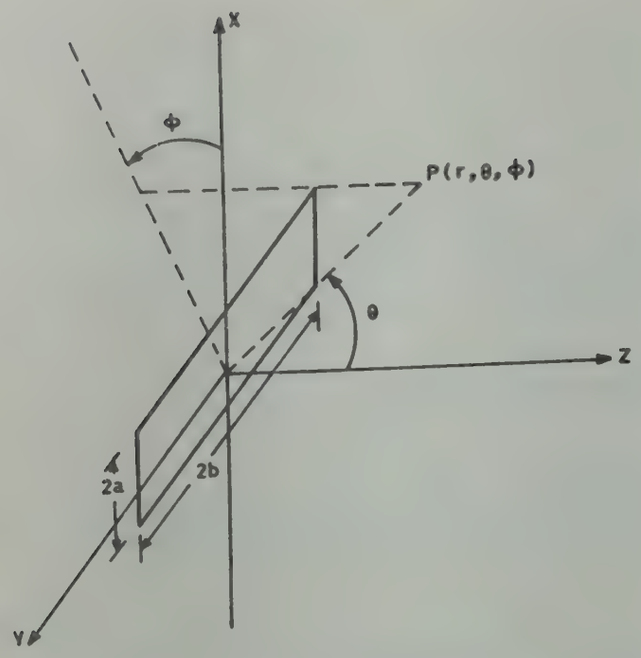

Fig. 2—Geometry of a slot antenna

$$\mathbf{E}_e = -\frac{4j\mu_0 a E_0 w}{rb}\exp(jwt-\beta_e r)[M_2] \times(\cos\theta\sin\varphi\hat{\theta}+\cos\varphi\hat{\varphi}) \quad \ldots (7)$$

where

$$[M_2]=[M_1]\cos(2ka\cos\theta) \quad \ldots (8)$$

and $k=k_0\sqrt{\varepsilon_r}$. The image factor $\cos(2ka\cos\theta)$ is obtained[2] by assuming that the slot is imbedded in a half-space of dielectric constant ε_r.

The far zone electroacoustic field $\mathbf{E}_p$ is given by[3]

$$\mathbf{E}_p=\frac{e}{\varepsilon_0\beta_p^2}\nabla n_1 \quad \ldots (9)$$

where

$$n_1=\frac{1}{4\pi}\frac{w_p^2}{eV_0^2}\int_V\frac{\rho}{r}\exp(-j\beta_p r)\,dv \quad \ldots (10)$$

and

$$\rho=\pm j\frac{I}{w}\exp(jwt) \quad \ldots (11)$$

After some manipulation the value of $\mathbf{E}_{pr}$ is obtained as

$$\mathbf{E}_{pr}=\frac{16w_p^2\beta_p ab\,E_0}{w^3A^2\varepsilon_0 r}\sin\varphi[N]\exp\{j(wt-\beta_p r)\} \quad \ldots (12)$$

where $[N]=$

$$\left[\left\{\frac{\sin(\beta_p a\sin\theta\cos\varphi)\cos(\beta_p b\sin\theta\sin\varphi)\cos(\beta_p\frac{l}{2}\cos\theta)}{\cos\varphi(\pi^2-4b^2\beta_p^2\sin^2\theta\sin^2\varphi)}\right\} \times\cos(2ka\cos\theta)\right] \quad \ldots (13)$$

It may be mentioned here that the above field expressions for the electromagnetic and the electroacoustic modes are valid for homogeneous, unbounded isotropic plasma region. The free space expression are recovered when A is taken equal to 1 ($w_p=0$).

3 Field Pattern Factors

The EM and EA mode field pattern factors are related to the electric intensity as[7]

$$F=\frac{r}{240\,E_0}|E| \quad \ldots (14)$$

where

$$E_0=\pm\frac{Im}{4a} \quad \ldots (15)$$

and I_m is the maximum value of I.

The EM mode field patterns $F_{e\theta}$ and $F_{e\varphi}$ and the EA field pattern F_{pr} are obtained as

$$F_{e\theta}=16k_1k_2\lambda_0[D]\cos\theta\sin\varphi \quad \ldots (16)$$

and

$$F_{e\varphi}=16k_1k_2\lambda_0[D]\cos\varphi \quad \ldots (17)$$

where

$$[D]=\frac{\sin(2k_1A\sin\theta\cos\varphi)}{2\pi k_1A\sin\theta\cos\varphi}\times\frac{\cos(2\pi k_2A\sin\theta\sin\varphi)}{\{(4k_2A\sin\theta\sin\varphi)^2-1\}} \times\cos(\pi k_3A\cos\theta)\cos(4\pi k_1\sqrt{\varepsilon_r}\cos\theta) \quad \ldots (18)$$

$$k_1=\frac{a}{\lambda_0},\ k_2=\frac{b}{\lambda_0},\ k_3=\frac{l}{\lambda_0}\ \text{where}\ l=\frac{\lambda_0}{2}$$

and

$$F_{pr}=\frac{8}{\pi}\left(\frac{1-A^2}{A}\right)\left(\frac{c}{v_0}\lambda_0\right)k_2\sin\varphi[G] \quad \ldots (19)$$

where

$$[G]=\left[\frac{\sin[(c/v_0)2\pi Ak_1\sin\theta\cos\varphi]}{\cos\varphi\{1-[4(c/v_0)Ak_2\sin\theta\sin\varphi]^2\}} \times\cos\left(\frac{c}{v_0}k_3\pi A\cos\theta\right)\cos\left(4\pi k_1\sqrt{\varepsilon_r}\cos\theta\right)\right] \quad \ldots (20)$$

and

$$A^2=1-\frac{w_p^2}{w^2} \quad \ldots (21)$$

The computation of the field patterns using Eqs (16), (17) and (19) are made using advanced programmable calculating machine (DCM MOSCAL 1185) and making use of its programme library. In our calculations the value of c/v_0 is taken equal to 10^3.

4 Results and Discussion

The field pattern factors for the electromagnetic and the plasma mode are computed and plotted in Figs 3 to 7 for a practical case reported by James and Wilson[9]. The value of $k_1 = 0.05$, $k_3 = 0.5[k_3 = (l/\lambda_0)]$ and k_2 are taken as 0.25 and 0.5. The direction and magnitude of maxima for $F_{e\theta}$ and $F_{e\varphi}$ are shown in Table 1.

It may be noted from Eq. (18) that at $\varphi = \pi/2$ (YZ-plane) the values of $F_{e\varphi}$ and $F_{e\theta}$ become zero. To obtain the variation of $F_{e\theta}$, its value is computed at $\varphi = 89.99$ deg and after normalization, plotted in Figs 3 and 4. From Figs 3 and 4 and Table 1, we can see that the direction and intensity of maxima are affected by the presence of ionized medium. For $k_2 = 0.25$, with the increase in plasma frequency, the direction of maxima decreases in the first and third quadrants and increases in the second and fourth quadrants. However, for k_2

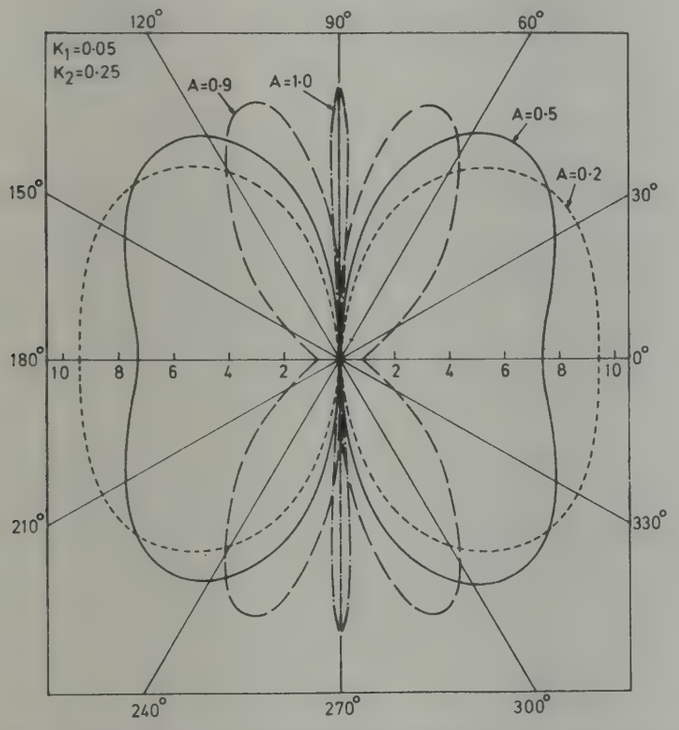

Fig. 3—Variation of normalized field pattern factor $F_{e\theta}(\varphi = 89.99)$ for $k_2 = 0.25$ at different plasma frequencies ($A = 0.2$, 0.5, 0.9 and 1.0)

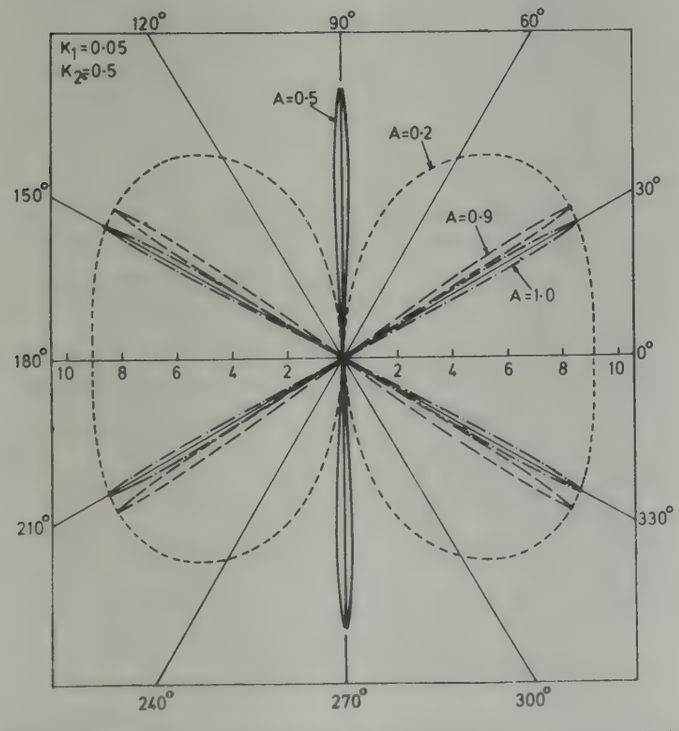

Fig. 4—Variation of normalized field pattern factor $F_{e\theta}(\varphi = 89.99)$ for $k_2 = 0.5$ at different plasma frequencies ($A = 0.2$, 0.5, 0.9 and 1.0)

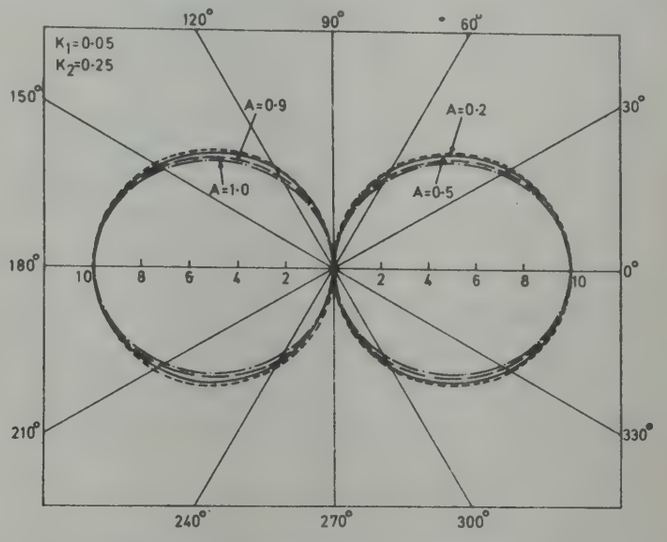

Fig. 5—Variation of normalized field pattern factor $F_{e\varphi}(\theta = \pi/2)$ for $k_2 = 0.25$ at different plasma frequencies ($A = 0.2$, 0.5, 0.9 and 1.0)

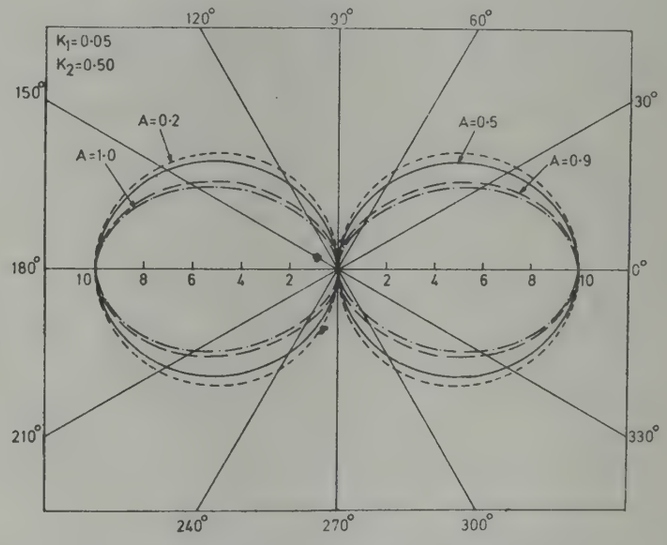

Fig. 6—Variation of normalized field pattern factor $F_e(\theta = \pi/2)$ for $k_2 = 0.5$ at different plasma frequencies ($A = 0.2$, 0.5, 0.9 and 1.0)

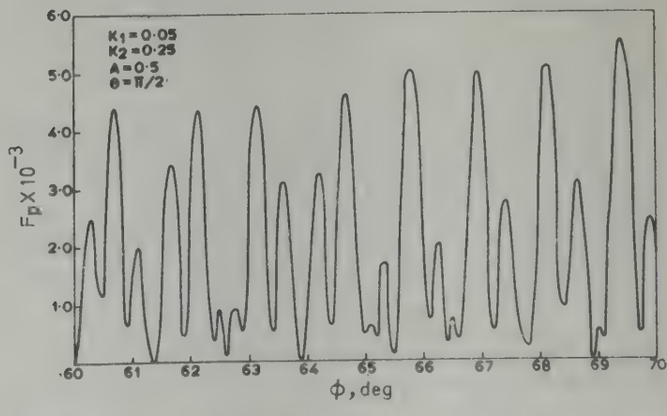

Fig. 7—Variation of F_{pr} for $k_2 = 0.25$ and $A = 0.5$ in $\theta = \pi/2$ plane

Table 1—Direction of Maxima and Magnitude of $F_{e\theta}$ at $\varphi=89.99°$ and $F_{e\varphi}$ at $\theta=\pi/2$ for $k_2=0.25$ and 0.5 for Various Plasma Frequencies

k_2	A	w_p/w %	$F_{e\theta}$ (E-plane); θ varies; $\varphi=89.99°$		$F_{e\varphi}$ (H-plane); φ varies; $\theta=\pi/2$	
			Directions of maxima	Maximum magnitude $\times 10^{-3}$	Direction of maxima	Maximum magnitude $\times 10^{-3}$
0.25	1.0	0	89.95°, 90.05°, 269.95°, 270.05°	9604.98	0°, 180°	1.7167610
0.25	0.9	43.6	71°, 111°, 249°, 289°	87.46	0°, 180°	1.7221673
0.25	0.5	86.6	49°, 129°, 231°, 311°	46.19	0°, 180°	1.7381607
0.25	0.2	98.0	30.5°, 150.5°, 209.5°, 329.5°	48.00	0°, 180°	1.7441817
0.5	1.0	0	29.5°, 150.5°, 209.5°, 330.5°	663.23	0°, 180°	3.433522
0.5	0.9	43.6	33.5°, 146.5°, 213.5°, 326.5°	2895.45	0°, 180°	3.444334
0.5	0.5	86.6	89.95°, 90.05°, 269.95°, 270.05°	19210.82	0°, 180°	3.4763214
0.5	0.2	98.0	40.5°, 139.5°, 220.5°, 319.5°	100.76	0°, 180°	3.488362

$=0.5$, the direction of maxima in the first and third quadrants first increases and then decreases sharply whereas for the second and fourth quadrants the case is reverse. For both the cases, it is observed that lobes become flattened with increase in plasma frequency.

In the XY-plane ($\theta=\pi/2$), $F_{e\theta}$ is zero and the normalized variation of $F_{e\varphi}$ is shown in Figs 5 and 6. From Table 1, it is noted that maximum amplitude and direction of maxima remain same for different plasma frequencies. However, the size of lobes for $k_2=0.25$ and 0.5 increases with increasing plasma frequencies. This can be explained by noticing the marked variation in maximum intensity in $F_{e\theta}$ which may be redistributed in $F_{e\varphi}$ with increasing plasma frequency. For $k_2=0.25$ this redistribution is very small. The free space $F_{e\varphi}$ patterns are obtained by substituting $A=1$. It may be mentioned that these are similar to the one experimently obtained by Derneryd[10].

On an inspection of F_{pr}, it is noted that there should be several hundred maxima and minima due to occurrence of c/v_0 in the expression of the pattern factor F_{pr}. In fact, this is confirmed by plotting amplitude at 0.1-deg interval from 60° to 70°. There are about 20 lobes in this interval. This is plotted in Fig. 7 for $k_2=0.25$ which shows a diserete ray-like structure for this mode. The intensity of plasma mode field patterns is found to be much less compared to the EM mode.

5 Conclusion

From Figs 3 to 7 and Table 1, it can be concluded that due to the excitation of electroacoustic mode, the field patterns of the microstrip line antenna are greatly modified. Two of the possible reasons for this are (i) the change in the propagation constant for the source current and (ii) the generation of the longitudinal plasma waves. The main patterns in the XY-plane become more directive with increasing plasma frequency. In YZ-plane its intensity remains zero. However, a few minutes off YZ-plane, the field patterns are greatly affected by the presence of plasma. Since, some power goes in the EA mode, the net available power for communication purpose is reduced. Also, the direction and amplitude of the maximum radiation are modified by the presence of the plasma. As these antennas are used on space vehicles for communication purpose, these results are relevant and significant for space craft antenna design engineers. It may be worth mentioning here that no experimental data are so far available for microstrip antennas immersed in plasma medium. However, the theory used to develop and compute the radiation properties of the antennas in this paper has suitably explained the radiation properties of loop and dipole antennas fixed on satellites[4,7].

Acknowledgement

The authors are grateful to the Indian Space Research Organization, Bangalore, for providing a research grant for carrying out the present work.

References

1 Post R E & Stephenson D T, *IEEE Trans Antennas & Propag (USA)*, **29** (1981) 129.

2 Carver K R & Mink J W, *IEEE Trans Antennas & Propag (USA)*, **29** (1981) 2.

3 Wait J R, *Appl Sci Pt B (Netherlands)*, **11** (1965) 423.

4 Gupta R K & Freeston I L, *Int J Electron (GB)*, **35** (1978) 545.

5 Derneryd A G, *IEEE Trans Antennas & Propag (USA)*, **24** (1976) 846.

6 Collin R E & Zucker F J, *Antenna theory, Part I* (McGraw Hill Book Co Inc, New York), 1969, 560.

7 Freeston I L & Gupta R K, *Proc Inst Elect Eng (GB)*, **118** (1971) 633.

8 Stratton J A, *Electromagnetic theory* (McGraw Hill Book Co Inc, New York), 1941.

9 James J R & Wilson G J, *Microwaves Optics & Acoustics (GB)*, **1** (1977) 165.

10 Derneryd A G, *IEEE Trans Antennas & Propag (USA)*, **26** (1978) 532.

Indian Journal of Radio & Space Physics
Vol. 13, August 1984, pp. 129-134

A Study of Archimedean Spiral Array-Feed Impedances & Radiation Patterns

K K DEY & V RAMACHANDRA
Department of Physics, Banaras Hindu University, Varanasi 221 005

Received 19 *December* 1983

A theoretical analysis of feed impedances and far-field radiation patterns of Archimedean spiral array (ASA) [of the form $r=a(1-\varphi/2\pi m)$] has been made. The analysis is based on induced EMF theory assuming thin linear, center-driven, non-staggered half-wave dipole radiators. The effect of various parameters of the ASA, viz. (i) number of dipole radiators (N) (ii) number of spiral turns (m) and (iii) dimension of the spiral (a) on the feed inpedances and radiation patterns have been studied. A set of graphs, showing the variation of feed point resistances and reactances with radiator number and also the radiation patterns showing the effect of various parameters of the spiral array, have been plotted and discussed. In the vertical radiation pattern, a very sharp beam is observed about $\theta=0^{\circ}$ for the ASAs with horizontally placed half-wave dipoles arranged parallel to X-axis. It is concluded that by proper choice of array parameters and with proper excitation of the dipoles, the ASAs can be suitably used both for a 360° scanning and directional beaming.

1 Introduction

Antenna arrays, particularly circular and elliptical arrays, have been studied extensively for their utility in many system applications. The high resolution consideration of circular arrays[1] and concentration of the radiated power for ring arrays either in the plane of the ring or in the omnidirectional plane[2] were reported. Cheng and Tseng[3] considered the gain maximization problem of circular and elliptical arrays. However, the spiral arrays did not receive the attention they deserve. It is noteworthy to mention that the spiral arrays like circular and elliptical arrays have the capability of scanning a complete 360° range. Some work regarding the radiation patterns of the spiral arrays with isotropic point source radiators has already been done[4-6]. However, if half-wave dipole radiators are used instead of point sources, the radiation patterns will be effectively changed due to mutual interactions amongst the radiators[7].

In a recent work, a comparative study of feed impedances of a circular and three different spiral antenna arrays, viz. trigonometric, Archimedean and exponential-trigonometric spiral arrays has been done[8]. These array systems can be used in UHF range. It was shown that the feed impedance behaviour of the Archimedean spiral array (ASA) lies in between that of the trigonometric and exponential-trigonometric spiral arrays. Thus a detailed and systematic knowledge of the feed impedances of the half-wave dipole radiators and the radiation patterns of the ASA is necessary.

With the above aim in view, this paper deals with the numerical results of the feed impedances and radiation patterns of the ASA based on induced emf theory. For completeness of the study, various parameters of the ASA, viz. variation in radiator number ($N=5$, 10, 15 and 20), number of spiral turns ($m=1$, 2, 3 and 4) and dimension of the spiral ($a/\lambda=1$ and 2) were taken into consideration and their effects on feed impedances and also on radiation patterns were reported. The form of the Archimedean spiral is represented by $r=a(1-\varphi/2\pi m)$ where a is the dimension of the spiral and m is the number of turns. The ASA is assumed to have center-driven non-staggered, thin-linear half-wave dipole radiotors. Studies for the radiation patterns were made both for the cases when the dipole radiators are placed vertically parallel to Z-axis and also when they are placed horizontally parallel to X-axis. Though the theory holds good for infinitely thin, linear antennas, nonetheless it serves as a practical approximation of the ASAs with the antennas of finite thickness. The ground effect has been neglected for horizontally placed radiators.

2 Theoretical Analysis

The equation of the Archimedean spiral is given as

$$r=a(1-\varphi/2\pi m) \qquad \ldots (1)$$

where the notations have already been explained. Two representative diagrams of the section of ASA with single and four turns are shown in Figs 1(a) and 1(b), respectively. The dots in Figs 1(a) and 1(b) represent the positions of the twenty half-wave dipole radiators. In all the cases the radiators are arranged at a regular interval of azimuthal angle $\varphi=2m\pi/N$, where the pth radiator is placed at an angle $\varphi_p=2m\pi p/N$ from the X-axis.

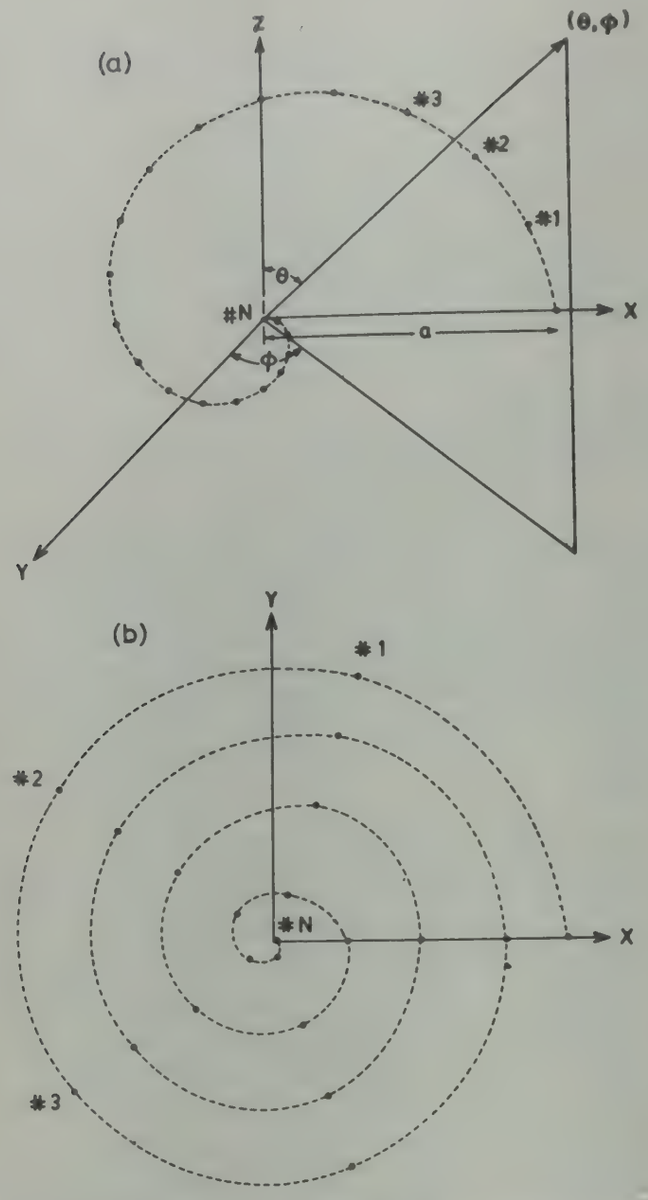

Fig. 1—(a) Geometry of the single turn, twenty radiator ASA (The points represent the respective positions of the half-wave dipoles); and (b) two-dimensional geometry of the four turn, twenty radiator ASA

The radiation pattern is determined by utilizing the well-known principle of pattern multiplication. It states that the far-field radiation pattern of a given array is given by the product of element factor and the magnitude of array factor, i.e.

$$E(\theta,\varphi)=|f(\theta,\varphi)|\,.\,|S| \qquad \ldots (2)$$

where $f(\theta,\varphi)$ is the element factor and S is the array factor. The element factor for vertically placed half-wave dipoles parallel to Z-axis may be written as

$$f(\theta,\varphi)=\cos(\pi/2\cos\theta)/\sin\theta \qquad \ldots (3)$$

Similarly, for horizontally placed half-wave dipoles parallel to X-axis, the dipole factor becomes

$$f(\theta,\varphi)=\frac{\cos(\pi/2\cos\varphi\sin\theta)}{\sqrt{1-\cos^2\varphi\sin\theta}} \qquad \ldots (4)$$

The array factor for the ASA can be written as[6]

$$S(\theta,\varphi)=\sum_{p=1}^{N} I_p\exp[jk_0\,a\sin\theta(1-\varphi_p/2\pi m)\times\cos(\varphi-\varphi_p)] \qquad \ldots (5)$$

In Eq. (5), I_p is the complex current of the pth radiator, k_0 is the free space propagation constant and $\varphi_p=2m\pi p/N$, where N is the total number of radiators. Hence,

$$E(\theta,\varphi)=\sum_{p=1}^{N} I_p\exp[jk_0\,a\sin\theta(1-\varphi_p/2\pi m)\times\cos(\varphi-\varphi_p)]\,.\,|f(\theta,\varphi)| \qquad \ldots (6)$$

From Eq. (6), the vertical radiation pattern may be obtained for different φ-planes. Similarly, the horizontal radiation pattern ($\theta=90°$-plane) becomes

$$E(90°,\varphi)=\sum_{p=1}^{N} I_p\exp[jk_0\,a(1-\varphi_p/2\pi m)\times\cos(\varphi-\varphi_p)]\,.\,|f(\theta,\varphi)| \qquad \ldots (7)$$

where

$$f(\theta,\varphi)=1 \text{ (for vertically placed dipoles)} \qquad \ldots (8a)$$

$$=\frac{\cos(\pi/2\cos\varphi)}{\sin\varphi}$$

(for horizontally placed dipoles) ... (8b)

A constant of proportionality in Eqs (6) and (7) is being dropped. The complex currents of the different radiators of the array must be evaluated for determining the radiation patterns. The matrix methods can now be used to evaluate the complex currents.

$$\begin{bmatrix} I_1 \\ \vdots \\ I_m \end{bmatrix}=\begin{bmatrix} Z_{11} & \cdots & Z_{1n} \\ \vdots & & \vdots \\ Z_{m1} & \cdots & Z_{mn} \end{bmatrix}^{-1}\begin{bmatrix} V_1 \\ \vdots \\ V_m \end{bmatrix} \qquad \ldots (9a)$$

or simply $[I]=[Z]^{-1}[V]$ ... (9b)

In Eq. (9b), $[I]$ and $[V]$ are the column matrices known as the current and the voltage matrices and $[Z]$ is a square matrix known as the impedance matrix. The vectors in the current matrix may easily be obtained once the specified voltage excitations of the radiators and the impedance matrix are known. From the knowledge of self and mutual impedances of the half-wave dipoles, the individual feed impedances of the radiators can be evaluated. The elements in the impedance matrix may be computed in the following way.

Assuming sinusoidal current distribution in the ratiator, the self-impedance of the pth half-wave dipole radiator simplifies to

$$Z_{pp}=(73+j42.5) \quad \text{ohm} \qquad \ldots (10)$$

Similarly, the mutual impedance between the pth and the qth half-wave dipole radiators may be obtained from the expression[8]

$$Z_{pq}=30[2\,Ci(k_0d_{pq})-Ci\{k_0[(d_{pq}^2+\lambda^2/4)^{\frac{1}{2}}+\lambda/2]\}-Ci\{k_0[(d_{pq}^2+\lambda^2/4)^{\frac{1}{2}}-\lambda/2]\}]$$
$$-j30[2\,Si(k_0d_{pq})-Si\{k_0[(d_{pq}^2+\lambda^2/4)^{\frac{1}{2}}+\lambda/2]\}-Si\{k_0[(d_{pq}^2+\lambda^2/4)^{\frac{1}{2}}-\lambda/2]\}] \quad \ldots (11)$$

where *Ci*s and *Si*s are the well-known cosine and sine integrals. The distance between the pth and qth radiators may be obtained from the geometry of the Archimedean spiral, i.e.

$$d_{pq}^2=a^2[(1-\varphi_p/2\pi m)^2+(1-\varphi_q/2\pi m)^2-2(1-\varphi_p/2\pi m)(1-\varphi_q/2\pi m)\cos(\varphi_p-\varphi_q)] \quad \ldots (12)$$

The analysis is carried out for a complete study of feed impedances and far-field radiation patterns of ASAs with vertically and horizontally placed half-wave dipoles.

3 Numerical Computations and Discussion of Results

A digital computer ICL 1904S has been used for the evaluation of d_{pq}s, Z_{pq}s, feed impedances and finally the radiation patterns of the array. The sine and cosine integrals of Eq. (11) are numerically computed with the help of the computer and are verified with the standard tables[9].

3.1 Variation of Feed Impedances and Radiation Patterns with Radiator Number

The variation of feed point resistances and reactances of the half-wave dipole radiators with radiator number ($N=5$, 10, 15 and 20) are shown in Figs 2 and 3, respectively. A single turn of the spiral with a fixed dimension ($a/\lambda=2$) has been considered in both Figs 2 and 3. It may be observed that both the graphs are of oscillatory nature and the undulations are more pronounced as the radiator number increases. When the number of radiators (N) is twenty, all the radiators show positive resistances except for the second radiator where a small negative resistance appears.

The variation of the vertical field amplitudes with θ for $\varphi=90°$-plane is shown in Fig. 4. The same parameters are retained in Fig. 4 as discussed in Figs 2 and 3. As expected, the nature of the field amplitudes for all the four cases is similar. When $N=20$, maximum field occurred at $\theta=40°$ with half-power beam-width angle of 22°. As usual, the field amplitude is minimum for all the cases at $\theta=0°$.

3.2 Variation of Feed Impedances and Radiation Patterns with Spiral Turns of the Array

Figs 5 and 6 represent the variations in the resistive and reactive parts of the feed impedances, respectively,

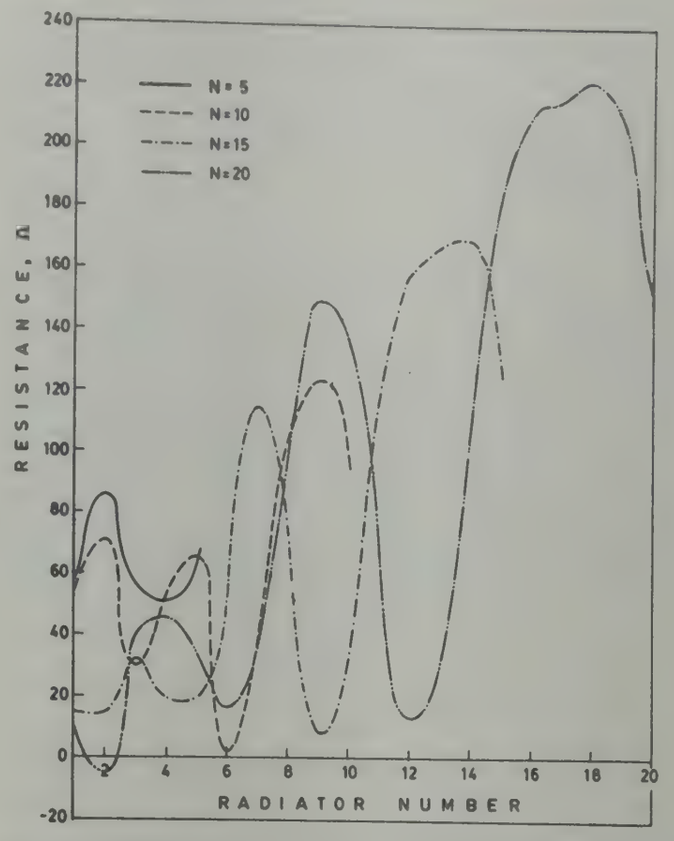

Fig. 2—Variation of resistive part of the feed impedances with radiator number ($a/\lambda=2$; $m=1$)

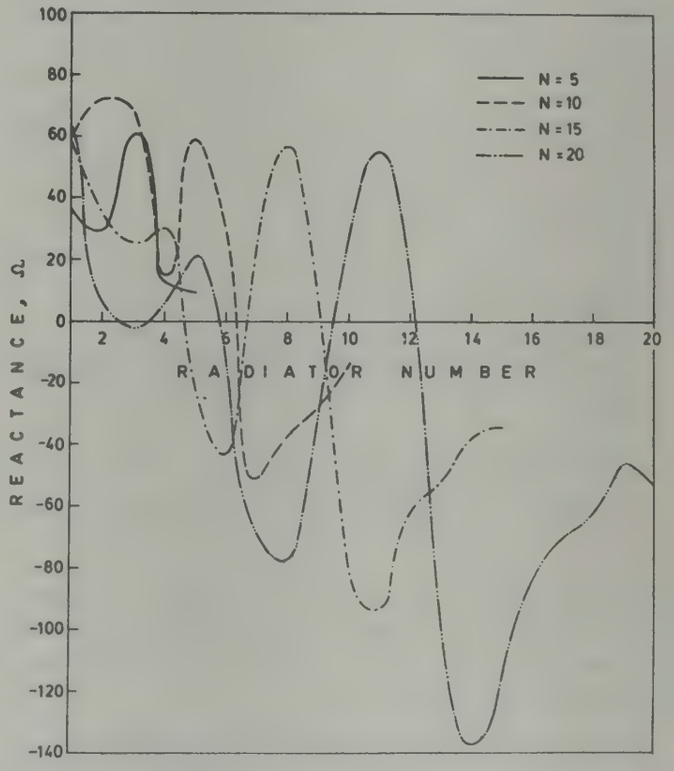

Fig. 3—Variation of reactive part of the feed impedances with radiator number ($a/\lambda=2$; $m=1$)

with the number of spiral turns of the array. The number of radiators in all the cases have been taken equal to twenty ($N=20$) and the array dimension has also been kept constant, i.e. $a/\lambda=2$. In both these graphs, periodic fluctuations occur. In Fig. 5, the maximum variation in the resistances occur between

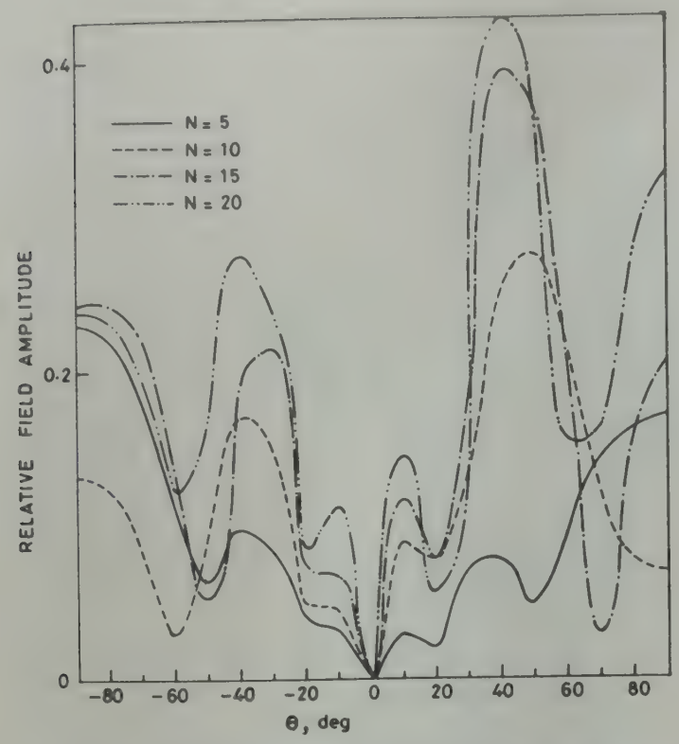

Fig. 4—Variation of the vertical field amplitudes with θ for different number of radiators ($a/\lambda=2$; $m=1$; $\varphi=90°$-plane)

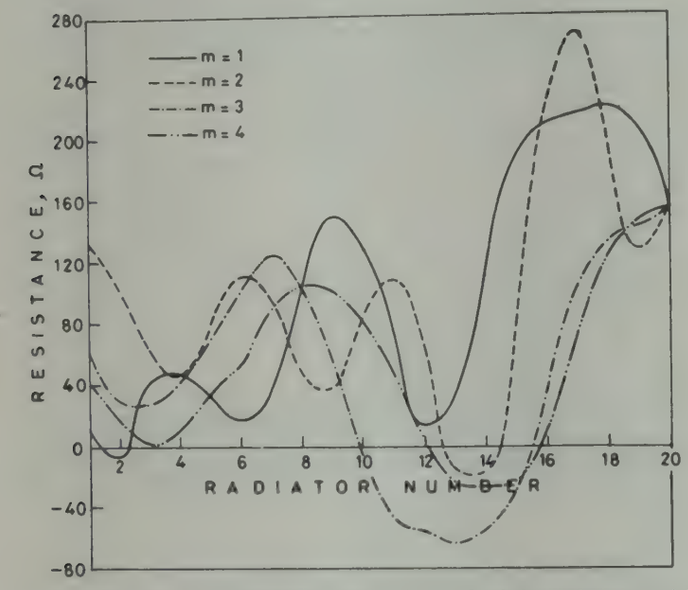

Fig. 5—Variation of resistive part of the feed impedances with radiator number ($a/\lambda=2$; $N=20$)

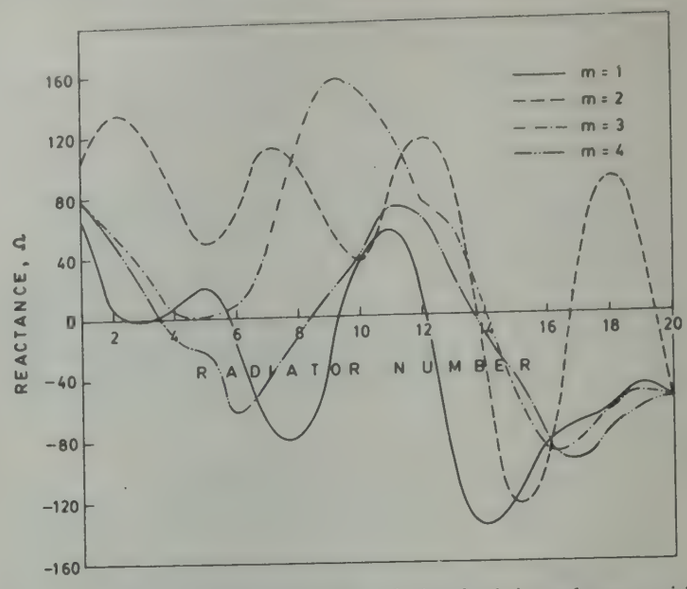

Fig. 6—Variation of reactive part of the feed impedances with radiator number ($a/\lambda=2$; $N=20$)

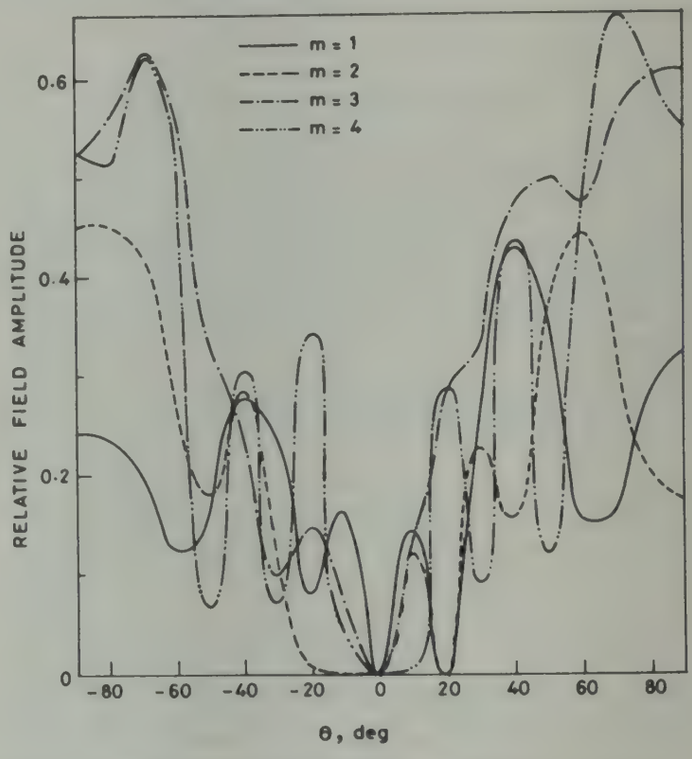

Fig. 7—Variation of the vertical field amplitudes with θ ($a/\lambda=2$; $N=20$; $\varphi=90°$-plane)

the fourteenth and the seventeenth radiators (approximately 290 ohms) for the spiral turns $m=2$. The least variation of the resistances (approximately 180 ohms) appear for $m=4$.

In Fig. 6, undulations in reactances occur for all the cases (i.e. $m=1, 2, 3$ and 4). As expected both capacitive and inductive reactances appear in Fig. 6. It is interesting to note that the maxima of the capacitive reactances appear to shift, in turn, from fourteenth, fifteenth, sixteenth and seventeenth radiators with the increase in spiral turns from $m=1$ to $m=4$, respectively.

The vertical and the horizontal radiation patterns for different spiral turns are shown in Figs 7 and 8, respectively. The other array parameters like dimension ($a/\lambda=2$) and the total number of radiators ($N=20$) are retained as in Figs 5 and 6. In both Figs 7 and 8, all the field amplitudes are normalized with respect to the maximum field amplitude obtained at $\varphi=220°$ for the case $m=3$ in the horizontal radiation pattern (Fig. 8). Further, it may be mentioned that in the other graphs, viz. Figs 4, 10 and 11, the field amplitudes are all normalized with respect to the same maximum field amplitude obtained at $\varphi=220°$ as mentioned earlier. In Fig. 7, the variation in field amplitudes are oscillatory in nature. The relative field amplitudes are drawn for $\varphi=90°$-plane. As expected, no symmetry can be observed with respect to $\theta=0°$. It

may be further observed that the field amplitudes increase with the increase in number of spiral turns.

The horizontal radiation patterns (Fig. 8) for all the cases i.e. $m=1$, 2, 3 and 4 are plotted against φ. The curves again exhibit oscillatory nature. The maximum field amplitude occurs at $\varphi=220°$ with HPBW of 32° for the case $m=3$. Another lobe with large amplitude is observed at $\varphi=80°$ with 87.5% of the field amplitude of the maximum.

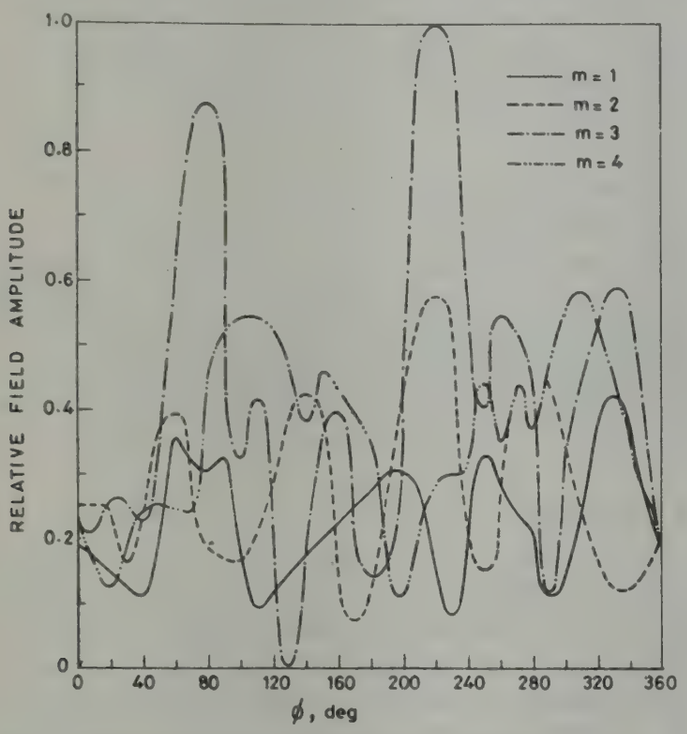

Fig. 8—Variation of the horizontal field amplitudes with φ ($a/\lambda=2$; $N=20$; $\theta=90°$-plane)

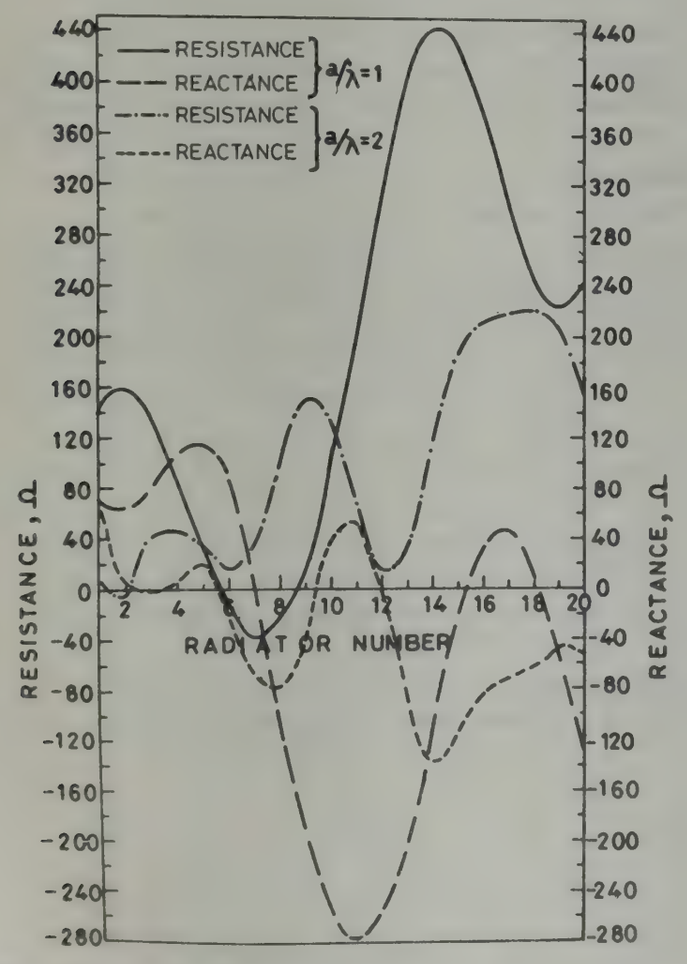

Fig. 9—Variation of resistive part/reactive part of the feed impedances with radiator number ($m=1$; $N=20$)

3.3 Variation of Feed Impedances and Radiation Patterns with Dimension of the Spiral Array

The variation of feed impedances (both resistances and reactances) with spiral array dimension ($a/\lambda=1$ and 2) is shown in Fig 9. For both the dimensions, a single turn ($m=1$) with twenty radiators ($N=20$) have been considered. It may be noted that for the spiral dimensions $a/\lambda=1$ and 2, the maximum resistances appear at fourteenth and eighteenth radiators, respectively. Both the resistive and reactive

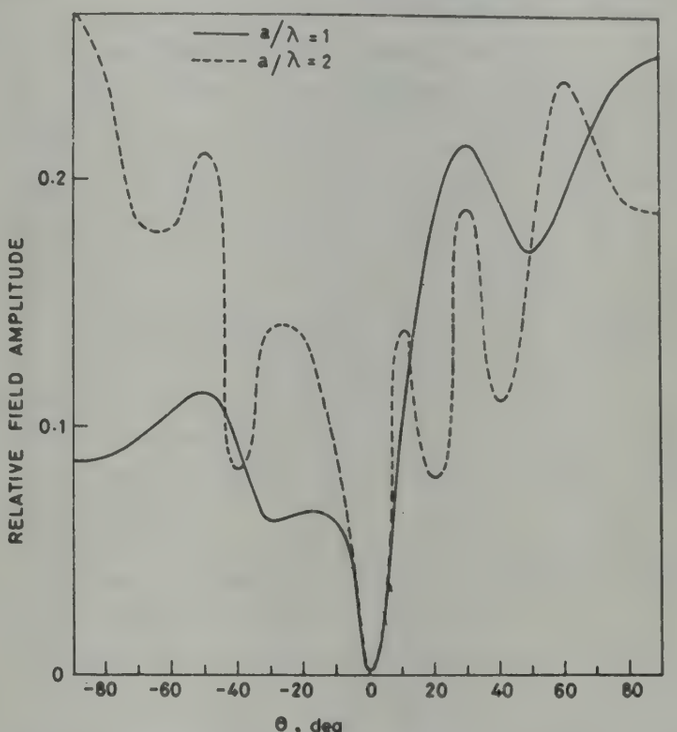

Fig. 10—Variation of the vertical field amplitudes with θ ($m=1$; $N=20$; $\varphi=90°$-plane)

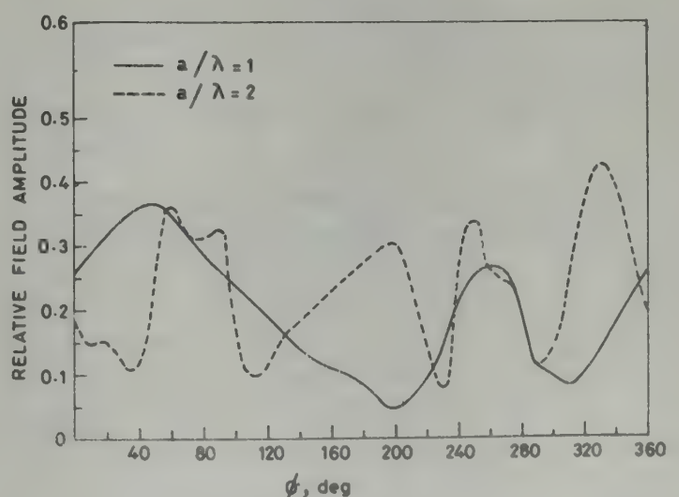

Fig. 11—Variation of the horizontal field amplitudes with φ ($m=1$; $N=20$; $\theta=90°$-plane)

components vary differently for the two different array dimensions. Thus, array dimension has an important role on the radiator feed impedance as other parameters of the array remain unchanged.

Fig. 10 shows the vertical radiation patterns with $\varphi = 90°$-plane whereas the horizontal radiation patterns are shown in Fig. 11. Again, to study this aspect, a single turn of the spiral ($m=1$) with twenty half-wave dipole radiators ($N=20$) for two-array dimensions, viz. $a/\lambda=1$ and $a/\lambda=2$ have been considered. It may be observed (Fig. 10) that a non-symmetry exists on either side of $\theta=0°$-plane, with a minimum field amplitude at $\theta=0°$. In Fig. 11, for both the dimensions of the array, undulatory response of the field amplitudes is observed.

3.4 Radiation Patterns with Horizontally Placed Half-wave Dipoles

In this case, the dipoles are placed parallel to X-axis. All the dipole radiators are placed along the Archimedean spiral path at a regular angular interval of azimuthal angle $\varphi = 2\pi m/N$, where the position of the pth radiator is determined by $\varphi_p = 2\pi mp/N$ from the X-axis. Out of many possibilities only one representative case, i.e. $a/\lambda=2$ and $N=20$ is discussed here for single and two turns of the spiral arrays. The resistances and the reactances of the half-wave dipoles in the array have already been presented in Figs 5 and 6, respectively.

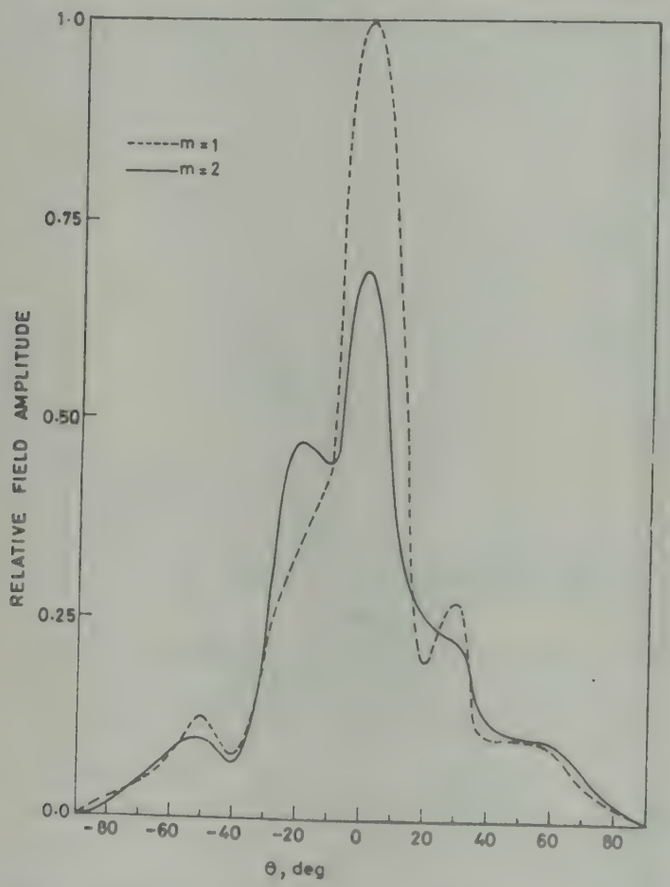

Fig. 12—Variation of the vertical field amplitudes for the ASA with horizontally placed half-wave dipoles ($a/\lambda=2$; $N=20$; $\varphi=0°$-plane)

The vertical radiation patterns for $\varphi=0°$-plane are computed using Eqs. (4) and (6) and are shown in Fig. 12. A sharp beam with HPBW angle of 18° at $\theta=0°$ is obtained for single-turn spiral array. A considerable side-lobe at $\theta=40°$ (57 %) is also observed for this case. For $m=2$, the maximum field amplitude is reduced to about 69 % (at $\theta=0°$) of that obtained for $m=1$.

4 Conclusion

By proper choice of array parameters and with proper excitation of the dipoles, one can obtain undulations in field amplitudes, flat regions and sharp beams too in the far-field patterns. Thus, ASA with half-wave dipole radiators can be suitably used both for a complete 360° scanning and for directional beaming.

Acknowledgement

One of the authors (V R) is thankful to the CSIR, New Delhi, for the award of junior research fellowship.

References

1 Wild J P, *Proc Roy Soc London Ser A*, **2** (1961) 84.

2 Royer G M, *IEEE Trans Antennas & Propag (USA)*, **14** (1966) 566.

3 Cheng D K & Tseng F I, *Proc IEE (GB)*, **114** (1967) 589.

4 Dey K K & Khastgir P, *Proc IRE (Australia)*, **32** (1971) 349.

5 Dey K K & Misra V C, *IEEE Trans Antennas & Propag (USA)*, **20** (1972) 512.

6 Misra V C, Basu D & Dey K K, *Indian J Radio & Space Phys*, **2** (1973) 51.

7 Ramachandra V & Dey K K, *J Inst Electron & Telecommun Eng (India)*, **29** (1983) 251.

8 Ramachandra V, Dey K K & Khastgir P, *Indian J Radio & Space Phys*, **11** (1982) 136.

9 *Handbook of Mathematical Funcations*, edited by M Abramowitz & I A Stegun (Dover Publications, New York), 1968, 238.

Indian Journal of Radio & Space Physics
Vol. 13, August 1984, pp. 135-136

Communications

Association of the Periods of Equatorial Pc4 & Pc5 Pulsations with Solar Wind Velocity

D R K RAO, G K RANGARAJAN & R L ASINKAR
Indian Institute of Geomagnetism, Bombay 400 005

Received 21 *December* 1983

Using longer period Pc4 and Pc5 pulsations from telluric current recordings made at Choutuppal (Hyderabad), a relation between the solar wind velocity and the period of pulsations is worked out. At this equatorial station, for pulsations in the period range from 100 to 300 sec, an increase in the period with increase in solar wind velocity is observed, and beyond an optimal velocity of $\simeq 550$ km/sec the periods decrease with increase in the velocity. This result is contrary to the inverse relation between periods and velocities reported for midlatitude stations.

Magnetic pulsations observed on ground may have source external to the magnetosphere or inside. Kelvin-Helmholtz instability excited by the flow of solar plasma along the flanks of the magnetosphere is one of the possibilities as a source mechanism for pulsations. Extra-magnetospheric origin of geomagnetic pulsations has been widely discussed in recent time[1,2]. Magnitude of interplanetary magnetic field (IMF) has been related to pulsation amplitude and period at midlatitudes by Vero[3] and for low latitudes by Rao[4]. Gul'yel'mi[5] showed that the main contribution to the variability in the Pc3 period is from the change in magnitude of the magnetic field ahead of the shock front. At middle latitudes, Gogatishvili[6] found that for IMF in excess of 5 nT with a southward orientation, Pc5 appears along with the main phase of storm. Gogatishvili[7] further showed a close relationship between the amplitude of longer period pulsations and parameters of IMF.

In pulsation studies, information from equatorial region has been sparse except for some recent work[8,9]. Relationship of pulsation period and amplitude at low latitude with the IMF parameters will be useful in discussing claims of different theoretical models for production and propagation of HM waves in the magnetosphere and ionosphere. In this communication, we show that a well-defined relationship exists between the solar wind velocity and the period of magnetic pulsations in Pc4 and Pc5 range at low latitudes.

The basic data are derived from the records of telluric current pulsations for the years 1968 to 1975 (both inclusive) at Choutuppal, Hyderabad (geomag. lat. 7.5°N). Mean period for each UT hour has been computed confining attention to only longer period Pc4 (100-150 sec) and Pc5 pulsations. Corresponding solar wind velocity data were taken from NASA compilation[10]. For examining the nature of the relationship between solar wind velocity and pulsation periods, the pulsation data were subdivided into 10 groups at 50-sec period interval (100-150, 150-200, ----, 550-600 sec). Mean solar wind velocity together with the standard error and median solar wind velocity with its upper and lower quartiles were computed for each of the 10 bins. Median values provide a better measure for the central tendency and are unaffected by a few relatively extreme values, if any. These are listed in Table 1, together with number of data points utilized in computation.

Plot of solar wind velocity and period of Choutuppal pulsation in the Pc4-Pc5 range is shown in Fig. 1. A third degree polynomial of the form

$$V = 22.75 + 4.34\,T - 0.01\,T^2 + (0.78 \times 10^{-5})\,T^3$$

between the period (T) and solar wind velocity (V) is found to fit the data very closely. The fitted curve is also shown in Fig. 1. Similar third degree polynomial with median velocities has also given more or less identical coefficients and hence these are not listed here. Both mean and median velocities have been used with small differences in the coefficients of the polynomial.

The most striking aspect of the solar wind velocity pulsation period relationship is the drastic change near the apex corresponding to periods of about 300-350 sec. While the pulsation period between 100 and 300 sec shows a near linear increase with solar wind velocity, the tendency just reverses with a very narrow transition region centred on $T = 300$ sec. The maximum solar wind speed corresponding to this is about 550 km/sec which is usually the velocity associated with high speed streams. It, therefore, appears to be an upper limit of the wind speed that can be directly related to (low latitude) pulsations.

Table 1—Variation of Mean and Median Solar Wind Velocity with Mean Period of Equatorial Pulsations

Period group sec	Total No. of observations for period and velocity	Mean period (T) sec	Mean velocity (V) km/sec	Standard deviation (σ)	Standard error (E)	Median velocity km/sec	Lower quartile	Upper quartile
100-149	1480	125	423	105	2.7	397	346	476
150-200	640	175	468	124	4.9	445	369	560
201-250	1325	225	557	128	3.5	568	385	726
251-300	1360	275	568	122	3.3	579	476	660
301-350	983	325	563	113	3.6	575	517	615
351-400	797	375	549	110	3.9	563	536	581
401-450	723	425	528	107	4.0	521	513	533
451-500	460	475	480	98	4.6	472	407	536
501-550	282	525	468	91	5.5	458	394	533
551-600	91	575	443	95	10.0	415	376	480

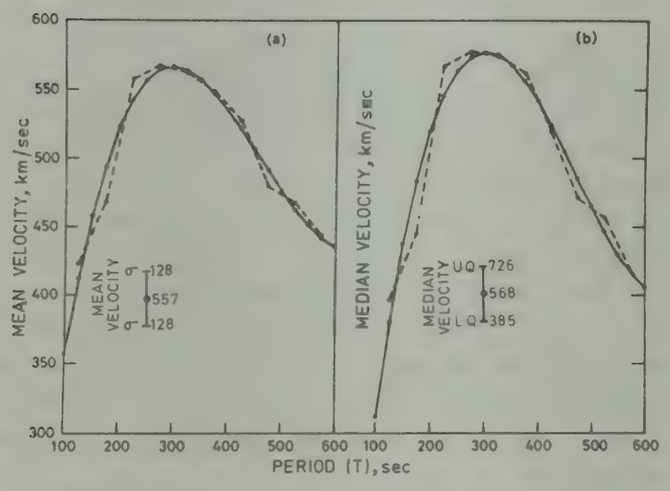

Fig. 1—Observed (----------) and computed (———) curves showing relation between pulsation periods and (a) mean solar wind velocity and (b) median solar wind velocity [Maximum standard deviation with respect to mean velocity is indicated in Fig. 1(a) and maximum upper and lower quartiles with respect to median velocity is shown in Fig. 1(b).]

Recently, Gogitishvili *et al.*[11], based on the pulsational data from high latitude stations in the USSR region, have shown that the dependence of Pc5 period during stormtime on solar wind velocity is non-linear and an empirical relation of the form

$$\log T = 5.542 - 1.01 \log V$$

will explain the distribution. In deriving the above relation, they have used the ground base data for the years 1968 to 1973 covering pulsation periods from less than 200 to 1000 sec. The relation worked out for the equatorial station in this communication is also for the same interval of years which, however, has shown a definite reversal in trend at about 300-sec period corresponding to the velocity of 550 km/sec; the pulsations, however, are not classified as stormtime or otherwise.

From the fact that Pc5 were observed simultaneously in the interplanetary medium and on surface and from the close relationship between IMF and longer period pulsations during magnetic disturbances at middle latitudes, Gogitishvili[7] suggested that Pc5 with periods greater than 300 sec can arise from beyond the boundary of the magnetosphere. It is remarkable that the transition period, as seen in Fig. 1 for equatorial pulsation relationship with solar wind speed, is also close to 5 min.

References

1 Gul'yel'mi A V, *Space Sci Rev* (*Netherlands*), **16** (1974) 331.
2 Russell C T & Fleming B K, *J Geophys Res* (*USA*), **81** (1976) 5882.
3 Vero J, *Proceedings of the international workshop on selected topics of magnetospheric physics, Tokyo*, 1979, 177.
4 Rao D R K, *Proceedings of the international workshop on selected topics of magnetospheric physics, Tokyo*, 1979, 150.
5 Gul'yel'mi A V, *Geomagn & Aeron* (*USA*), **13** (1973) 105.
6 Gogatishvili Ya M, *Geomagn & Aeron* (*USA*), **14** (1974) 767.
7 Gogatishvili Ya M, *Geomagn & Aeron* (*USA*), **16** (1976) 225.
8 Rao D R K, Asinkar R L, *Proceedings of the symposium on interdisciplinary approaches to geomagnetism held at Indian Institute of Geomagnetism, Bombay*, 1981, 305.
9 Sarma Y S, Sastri T S, Sanker Narayan P V & Sarma S V S, *J Geomag & Geoelect* (*Japan*), **33** (1981) 341.
10 King J W, *Interplanetary Medium Data Book* (*USA*), NSSDC/WDC-R & S-77-40, NASA, 1977.
11 Gogatishvili Ya M, Metonidze T V & Kereselidze Z A, *Geomagn & Aeron* (*USA*), **20** (1980) 248.

Indian Journal of Radio & Space Physics
Vol. 13, August 1984, pp. 137-138

A Circularly Polarized Corrugated Flanged Feed Horn— Its Design & Development

P MOHANAN, C K AANANDAN & K G NAIR
Department of Electronics, University of Cochin, Cochin 682022

Received 19 *April* 1984

Design and development of a circularly polarized and matched *H*-plane sectoral horn antenna have been reported. By proper trimming of the flange parameters, any desired polarization can be obtained from the horn.

Pioneer workers[1-3] explored certain conditions for producing circular polarization, tilt of polarization, etc. for beams from reflection grating with metallic corrugated walls. The aim of the present study is to design and develop a circularly polarized *H*-plane sectoral horn antenna using corrugated flange technique. These may find practical applications in communication satellite, radar, etc.

Geometry of the flanged horn is shown in Fig. 1. Aluminium is selected for the fabrication of the flanges as it offers good conductivity, low cost and minimum weight. The experiment is conducted with corrugated comb profiles having depths varying from 0.109λ to 0.140λ, and corrugation periods varying from 0.110λ to 0.385λ, where λ is the free space wavelength. The corrugations are inclined at 45° to *E* vector component parallel to the plane of the flange. Depending upon the position of the flange from the aperture (Z), the flange angle (2β) and frequency (f), the desired polarization can be synthesized. This technique can produce a narrow pencil beam from the horn.

Polarization pattern in the *H*-plane of the flanged horn is plotted by rotating a distant linearly polarized antenna. The radiation patterns in the co-polar and cross-polar planes are recorded in the usual manner with flanged horn as the transmitter. The VSWR of the system is also studied using the normal test bench method. These experiments were done inside an anechoic chamber.

The variations of the axial ratio along the on-axis with the position of the flange from the aperture of the horn (Z) are shown in Fig. 2. It is clear that there is a critical position for achieving a circular polarization. Generally, the pattern is elliptically polarized. By measurement of VSWR, it is observed that the matching condition also is improved at this critical position. In this case, at 9.345 GHz the VSWR with and without flanges are 1.32 and 1.53, respectively. The radiation patterns in the co-polar, cross-polar and 45° planes for the above system are presented in Fig. 3.

The on-axis axial ratio of the system is 0.268 dB. Typical radiation pattern having predominant cross-polarization is shown in Fig. 4. Typical radiation patterns monitored by left and right hand helical antenna are shown in Figs 5 and 6. It is interesting to note that when the tilt of corrugation is 45° as shown in Fig. 5 the sense of rotation is left and when the tilt angle

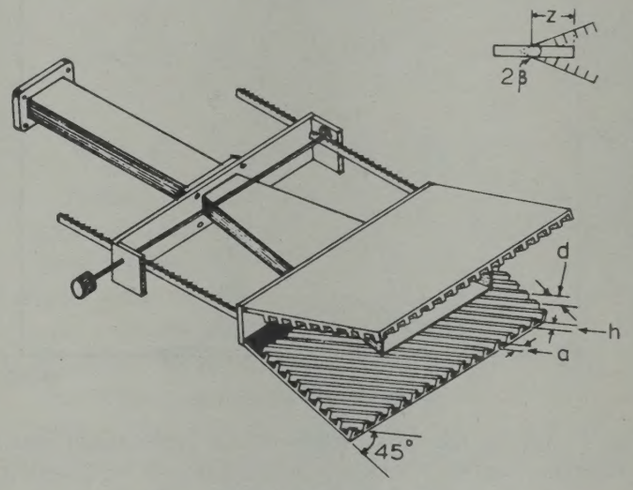

Fig. 1—Geometry of the flanged *H*-plane sectoral horn

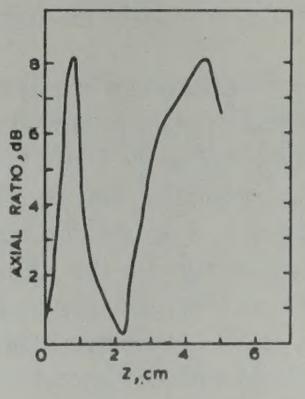

Fig. 2—Variation of axial ratio with the position of the flange from the aperture (Z) (Flanges with corrugation parameters $d = 0.1875\lambda$, $a = 0.156\lambda$, $h = 0.125\lambda$ and flange angle $2\beta = 45°$; horn length = 23.5 cm, *H*-plane width = 10 cm and flare angle = 24°, $\lambda = 3.2$ cm)

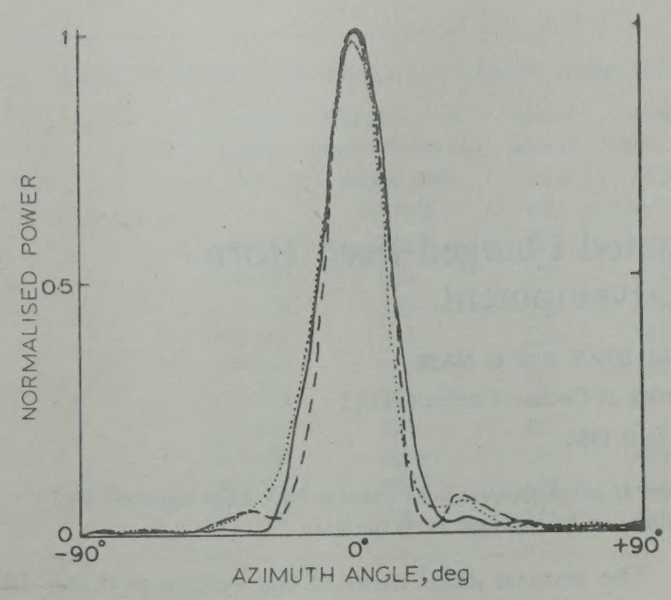

Fig. 3—Typical radiation pattern in different planes with Z = 2.2 cm and λ = 3.2 cm (———, Co-polar; ----, Cross-polar; and ...45° plane)

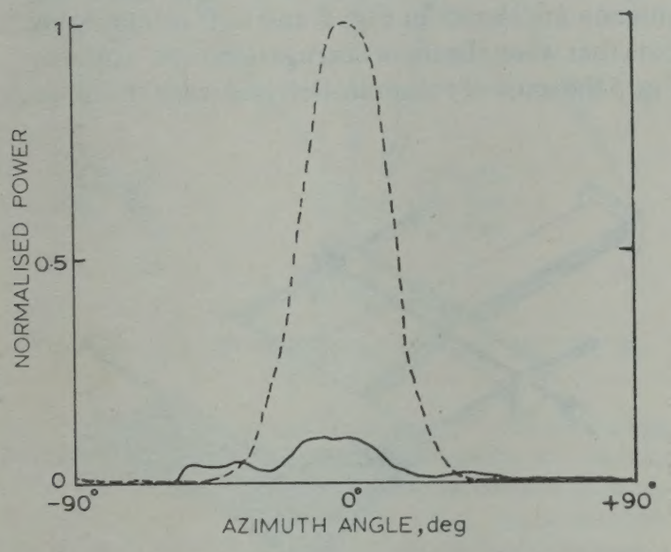

Fig. 4—Typical radiation pattern having predominant cross-polarization for Z = 4.5 cm and λ = 3.2 cm (———, Co-polar; and ---, Cross-polar)

is 135° (Fig. 6) it is circularly polarized in the right-hand sense.

The experimental results can be physically explained as follows. The incident plane polarized wave originated from the horn is inclined at 45° to the corrugation. This wave on the groove surface can be resolved into *TE* and *TM* components[1]. The tips of the corrugation will act as secondary radiators for the *TE* components and are totally reflected from the top of the corrugation. The other component is reflected from the bottom of the corrugations. At a particular value of Z, these two components and radiation from the horn may produce two equal and orthogonal components with phase quadrature which results in circular polarization. Here, it is observed that for a particular depth we can produce circular polarization at different wavelengths by proper adjustment of the other flange parameters.

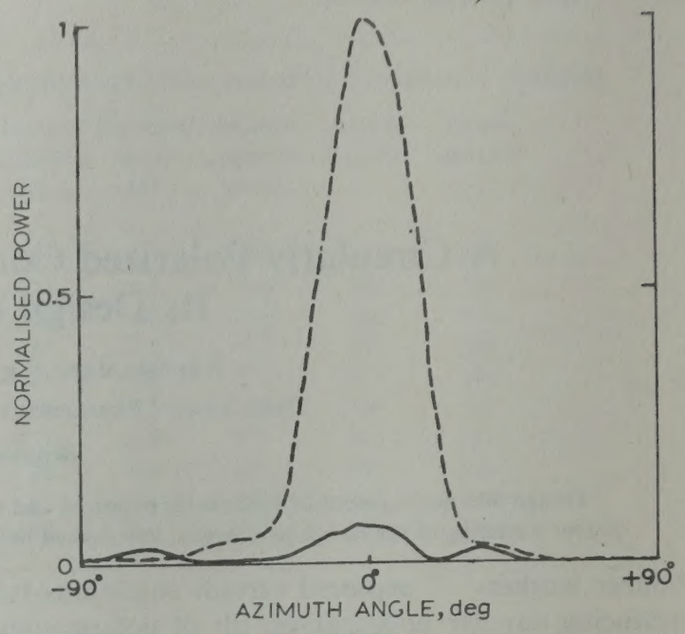

Fig. 5—Radiation pattern monitored by the helical antennas when the tilt of corrugation was 45° (———, Right-hand helical antenna; and ---, left-hand helical antenna)

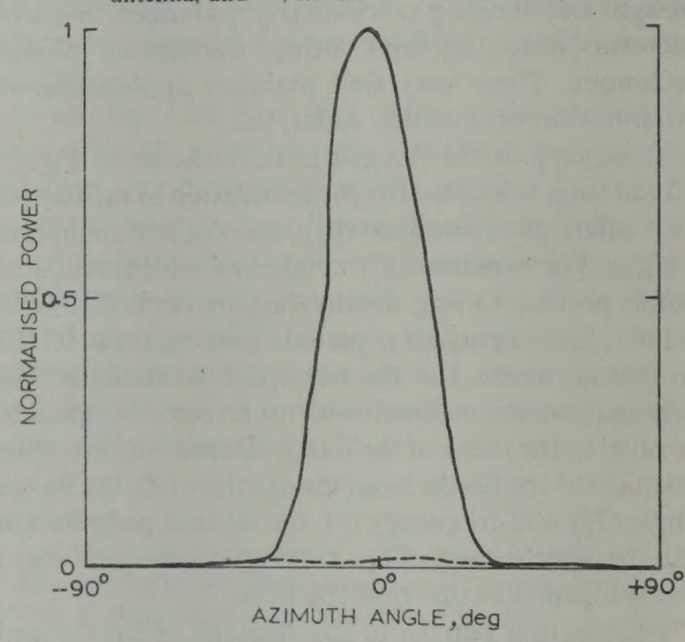

Fig. 6—Same as Fig. 5 but for 135° tilt

From the experiment, the optimum periodicity for fairly good circular polarization is in the range $\lambda/8$-$\lambda/4$. The main advantage of this type of antenna is that adjustment could be done readily to produce any desired polarization.

One of the authors (CKA) acknowledges the Council of Scientific and Industrial Research, New Delhi, for providing financial assistance. The authors wish to thank Prof. K Sathianandan, Head of the Department of Physics, University of Cochin, Cochin, for helpful discussion.

References

1 Jull E V, *Electron Lett (GB)*, **15** (1979) 423.

2 Ramsay J F, *Proceedings of conference on CW antennas for marine navigational radar held in London*, 1950, 24.

3 Paul P O & Nair K G, *Electron Lett (GB)*, **18** (1982) 338.

INSTRUCTIONS TO CONTRIBUTORS

General

Contributions should reflect original work done. They should neither have been published already nor be under consideration for publication elsewhere. The manuscripts should be typewritten only on one side of good quality thesis paper, in double space and with adequate margin on all four sides of the text matter. The original and two copies thereof, all the copies complete in all respects including abstract, figures, etc., are to be submitted.

Contributions should clearly bring out the justification for undertaking the investigation and outline the exact scope of the study. Elaborate and long introductions should be avoided. Minimum essential experimental details which would enable anyone to repeat the work, should be included. Accuracy of measurements, and limitations of the results and conclusion should be clearly stated. Discussion should be limited to the strictly essential and should not repeat lengthy statements of facts/observations, which are obvious from the tabular and graphical data presented. A separate section on 'Conclusions' can be included only when they are of outstanding significance. Mere observation of trends of results should be distinguished from firm conclusions. References given at the end should be strictly limited to the essential minimum. Large-scale reproduction of all references given in another single source should be avoided unless highly relevant.

Papers must be written in clear and concise English. Good attention to spelling and grammar should be given. Long introduction should be avoided. Stanadard international nomenclature should be followed in giving names of chemical compounds. Standard abbreviations for units of measurement should be used in the text, tables and illustrations. The abbreviations should be used without fullstops.

Title—The title should be neither too brief/general nor unnecessarily long. It should reflect the content of the paper so as to derive the maximum advantage in indexing and information retrieval. A short title for use as running title should also be supplied. If a paper forms part of a series, a subtitle indicating the aspects of the work covered in the paper should be provided.

Abstract—The abstract should indicate the scope of the work and the principal findings of the paper. It should not exceed 3% of the length of the paper and, barring exceptional cases, it should not exceed 200 words. The abstract should be prepared in such a form that abstracting periodicals can use it without modification.

The abstract including the title of the paper, authors' names and affiliations, a short running title and relevant footnotes, if any, should be typed on separate sheet.

Data—Only such primary data as are essential for understanding the discussion and the main conclusions emerging from the study should be included. All such secondary data as are of interest to a specific category of readership may, if necessary, be deposited in the editorial office (or retained by the authors) for supply on demand. A footnote to this effect may be inserted at a suitable place in the paper.

Mathematical Portions—Special attention should be given to the mathematical portions of the paper. Equations must be well separated from the text and written clearly with good separation between the successive lines. The usual norms of breaking long mathematical expressions may be adhered to. Equations should be numbered consecutively in Arabic numerals with the number in parentheses near the right hand margin. Superscripts and subscripts should be clearly indicated in pencil by V and Λ signs, respectively. Capital and small letters, particularly of the same letter when both occur, as well as letters or symbols likely to be confused one for the other, should be clearly distinguished. Special characters (e.g. Greek, Script, vector, tensor, matrix, etc.) required must be indicated by marginal notes. Letters and symbols which should appear in bold face must be clearly indicated. To simplify typesetting: (i) long and complicated mathematical expressions which are frequently repeated should be replaced with single letter/symbol, without clashing with the others used in the paper; (ii) the "exp" form of complex exponential functions should be used; and (iii) to simplify fractions, the solidus (/) is to be used and fractional exponents are to be used instead of root signs, e.g.

write $\left[4\omega_{pl} K_{3\lambda}^2 \Big/ \left(\tilde{\omega} K_D^2\right)\right]^{1/2}$ and *not* $\sqrt{\dfrac{4\omega_{pl} K_{3\lambda}^2}{\tilde{\omega} K_D^2}}$

write $\exp\{-i\omega_0 (t_1 - t_2)/2\}$ and *not* $e^{-i\omega_0 (t_1 - t_2)/2}$

Tables—Tables should be typed *on separate sheets* of paper without any text matter on the page. They should be numbered consecutively in Arabic numerals and should bear brief titles. *Column headings should be brief.* Units of measurement should be abbreviated and placed below the headings. Nil results should be indicated and distinguished clearly from absence of data. Presentation of the same data both in the form of tables and graphs should be avoided. Inclusion of structural formulae inside the tables should be avoided as far as possible. Tables should be referred to in the text by numbers and not by terms like 'above', 'below', 'preceding' or 'following'.

Illustrations—All illustrations must be numbered consecutively in Arabic numerals. Captions and legends to the figures should be self-explanatory and should be typed on a separate sheet of paper and attached at the end of the manuscript. Line drawings should be made with Indian ink on white drawing paper (preferably Bristol board), cellophane sheet or tracing cloth. Histograms, probability variation curves, etc. may be prepared with hatched lines instead of thick black ink. In addition to the originals, a set of blue-prints or photostat copies should be sent. For satisfactory reproduction, the graphs and line drawings should be drawn to approximately twice the printed size.

The lettering should be uniform, preferably in stencil, so as to be *not less than 2 mm after reduction* widthwise to 3″ or 6″ as required. The size of geometrical shapes (used to distinguish different graphs), dots, lines, etc. should be sufficiently large to permit the necessary reduction without

loss of detail. In the case of *photographs*, prints *must be on glossy paper and contrasty*. If an illustration is taken from another publication, reference to the source should be given and prior permission secured. Illustrations should be protected by thick cardboard packing against creases, folds and broken corners during transit. Illustrations should be referred to in the text by numbers and not by terms like 'above', 'below', 'preceding' or 'following'.

Spectra, ionograms, echograms, etc. should be included only if they are essential to the discussion; otherwise only significant numerical data should be included in the text.

References—The list of references should be prepared strictly in accordance with the style followed in the journal. In the text, references to literature should be numbered consecutively, in the order of their first occurrence, and should be indicated by superscripts at the relevant places; as far as possible the placement of references on numerals or other symbols should be avoided; in such cases the reference may be given in parenthesis in running text, e.g. "this yielded for n a value of 2.3 (Ref. 5)". Full bibliographic details for all the references mentioned in the text should be listed in serial order at the end of the paper.

In citing references to research papers, names and initials of authors should be followed, in order by the title of the periodical in the abbreviated form (underlined), the volume number (two lines underneath), the year within parenthesis and the page reference [e.g. Rastogi R G, *Indian J Radio & Space Phys*, **9** (1980), 173.]. For names of periodicals, the abbreviations followed by the *Physics Abstracts* should be used. For periodicals not covered by *Physics Abstracts*, the title abbreviations should be according to the *Bibliographic Guide for Editors and Authors*, 1974, published by the American Chemical Society, Washington DC, USA; additionally the country from which the journal is published should be given in parenthesis immediately after the title abbreviation. If a paper has been accepted for publication, the names of the authors and the journal should be given followed by the words "in press" [e.g. Mitra A P, *J Atmos & Terr Phys (GB)*, **37** (1975), in press.].

In the list of references, unpublished work, accepted papers in press and personal communications should be clearly distinguished.

Even if a reference contains more than two authors, the names of all the authors with their respective initials should be given. The abbreviations *et al.*, *idem* and *ibid* should be avoided.

Reference to a book should include, in the following order: names and initials of authors, the title of the book (underlined), name of publisher and place of publication within parenthesis and year [e.g. Smylie D E, Clarke G K C & Ulrych J J, *Methods in computational physics* (Academic Press Inc., New York), 1973, 391.]. If the reference is to the work of an author published in a book by a different author or edited by a different person, the fact that it is cited from the source book should be clearly indicated [e.g. Culhane J L, cited in *Supernovae*, edited by D N Schramm (D Reidel), 1977.].

Proceedings of conferences and symposia should be treated in the same manner as books. Reference to a paper presented at a conference, the proceedings of which are not published, should include, in the following order, names and initials of authors, title of the paper (underlined), name of the conference, place where the conference was held and date (Sen A K & Trehan S K, *Field changes of the sky wave component due to a local broadcast signal during different geophysical phenomena*, Paper presented to the Symposium on Earth's Near Space Environment, National Physical Laboratory, New Delhi, 18-21 Feb. 1975).

Reference to a thesis should include the name of the author, title of the thesis (underlined), university or institution to which it was submitted and year of submission (e.g. Burg J P, *Maximum entropy spectral analysis*, Ph D thesis, Stanford University, California, 1975.).

Reference to a patent should include names of patentees, country of origin (underlined) and patent number, the organization to which the patent has been assigned within parenthesis, data of acceptance of the patent and reference to an abstracting periodical where available [Labes M M, *US Pat.* 4,066,567 (to Temple University), 3 January 1978; *Chem Abstr*, **88** (No.20)(1978), 138350 n.].

Abbreviations, symbols and units—These should conform to the style of the journal.

Frequently repeated combinations of words, e.g. sudden ionospheric disturbance (SID), point discharge current (PDC), gradual rise and fall (GRF), etc. should be abbreviated subsequently, indicating the abbreviated form in parenthesis, as shown, at the place of their first occurrence.

Nomenclature—Where too many symbols are used in the text, a section entitled 'Nomenclature', explaining the significance of the various symbols, may be given and placed just above the Acknowledgement section.

Acknowledgement—Acknowledgements should not be exuberant and must be made only to real assistance rendered in connection with the scientific work reported in the paper.

Appendixes—Appendixes, typed on separate sheets, should be numbered consecutively, in Arabic numerals, in the order of their occurrence in the text, and should be placed at the very end of the paper.

Printed and Published by Shri D.S. Sastry, Publications & Information Directorate (PID), Council of Scientific & Industrial Research, New Delhi, at PID Photocomposition-cum-Printing Unit.